Conditional Stability of a Steam Jet during Direct Contact Condensation in Subcooled Water Crossflow

By

Max Brennan

A thesis submitted in partial fulfillment of the requirements for the degree of

Master of Science

(Mechanical Engineering)

At the University of Wisconsin-Madison

2018

Abstract

Direct condensation of steam in liquids is used in industrial applications as an efficient process heating technique. Direct contact condensation heaters have a smaller footprint than plate and frame heat exchangers used in similar applications and have fewer issues with fouling. At certain conditions of the liquid and steam the process becomes unstable and dangerous. The steam condensation produces damaging noise and pressure fluctuations in the liquid with high frequency (3-8 kHz). This thesis details an experimental investigation into the causes of condensation noise and how the frequency of pressure fluctuation changes with the liquid temperature and flow rate. It was found that oscillation frequency is high (8 kHz) and the steam jet is stable at cold liquid temperature. Frequency decreases with increasing liquid temperature until the steam jet becomes unstable and forms bubbles that collapse at a lower frequency (2-4 kHz). The bubble collapse creates noise several orders of magnitude higher than stable steam jet condensation. The steam condensation is unstable due to the imbalance in the rate of steam supplied through the nozzle and the rate of steam condensed into the liquid.

Acknowledgements

Thank you first and foremost to my wonderful wife Meg for supporting me through the ups and downs of graduate school. Your boundless patience, kindness, and encouragement are the reason I could do this. Thank you to my parents and family for their love and encouragement throughout my life and providing me with opportunities to succeed.

Thank you to all of my friends in the SEL and MFVAL. The “extra-curricular” outings to football games, summer volleyball league, and frequenting adult beverage establishments provided some truly fun times.

Thank you to my advisors Greg Nellis, Arganthael Berson, and Kris Dressler for your advice and encouragement throughout the project. Also, thank you to Jim Zaiser and Hydro-Thermal Corporation for funding the project as well as Shawn Berg for the helpful guidance and advice.

All my best,

Max Brennan

Table of Contents

Table of Figures

Table of Tables

1. Introduction

Direct contact condensation is a technique used in industrial liquid heating applications and nuclear power plant pressure relief safety systems. Direct contact condensation is novel because the process directly mixes steam with the liquid to be heated, compared with common heat exchangers that transfer energy through a barrier. Direct contact condensation utilizes the latent and sensible energy present in the steam. Most heat exchangers only transfer the latent heat of the steam. Steam condensate must be returned to the boiler to be reheated and energy losses can occur. Direct contact condensation heaters avoid some common problems encountered when using conventional plate and frame heater exchangers including clogging when heating slurries and fouling due to buildup of baked on substances.

In many applications steam injection is fairly straightforward and only simple calculations are required which quantify steam mass input necessary to raise the temperature of the process liquid by the desired amount. However, in some cases the steam injection process creates an incredibly loud screeching noise that makes it uncomfortable and sometimes even dangerous for employees to work near the equipment when it is operating. The noise is generated by hydrodynamic pressure fluctuations that can also damage process control and measurement equipment. The behavior of the steam injection can be broadly defined to be quiet and “stable” vs. loud and “unstable” depending on the process conditions.

Many “regime maps” of direct contact condensation have been created which separate steam injection behavior into distinct regimes like chugging or condensation oscillation that are mapped to process parameters including steam mass flux and liquid

subcooling. It was found that the regime maps in the literature do not agree quantitatively with the results presented here, but qualitative trends are consistent.

This thesis focuses on understanding the behavior that creates noise in direct contact condensation and the transition from quiet to loud regime behavior. Understanding the transitionary behavior is critical to predicting the condensation regime at conditions that are not directly tested and for the design of equipment that can prevent or avoid undesirable behavior.

2. Background

Direct contact condensation has been extensively studied beginning in the 1970's and two major variations have been the focus of research: (1) injection of vapor into a quiescent pool of liquid and (2) injection of a vapor into flowing liquid. Most commonly the vapor and liquid are steam and water, but other applications including sodium vapor jet condensation have been studied [1]. The majority of the published research on direct contact condensation focuses on steam injected into quiescent pools of water. A type of safety cooling system in boiling water nuclear reactors rejects large amounts of heat from the reactor core by venting steam into water pools in an emergency event.

Kerney et al. was one of the first to complete a detailed, analytical study of sonic steam injecting into water in 1970. His work focused on correlating the jet penetration length with steam mass flux and condensation driving potential [2]. Many researchers after Kerney focused on aspects of direct contact condensation including jet penetration length, heat transfer coefficient, pressure oscillations, and mapping condensation regimes. Work was already performed in the Multiphase Flow Visualization and Analysis lab at UW-Madison in 2011[3] that focused on the jet penetration length and temperature distribution of steam injected into crossflowing water. Further discussion on those topics is not included in this thesis. The work presented here is focused on understanding condensation stability and pressure oscillation changes during the transition between regimes of condensation behavior.

This background section gives an overview of published literature on the two main topics of this thesis: (1) regime maps of condensation behavior and (2) pressure

oscillations created during the condensation process. An important consideration when analyzing published research is how drastically testing parameters and equipment geometry varies between experimental setups. Steam injection into pools is studied using nozzles oriented vertically downward, vertically upward, horizontally, or at various angles into pools of varying volume and through nozzles of varying diameter, length, and inlet geometry. Steam injection into flowing water is studied using nozzles oriented perpendicular to the flow, concurrent with the flow, or at various angles and through nozzles with varying diameters, lengths and inlet geometry. Due to the variations in test equipment the quantitative results from the literature generally did not agree well with the experimental data in this thesis. However, trends in oscillation frequency and magnitude found in the literature qualitatively matched the results presented in Chapter 7.

2.1.Regime Maps in Literature

A “regime map” is one of the common ways that data about direct contact condensation behavior is presented in the literature. A regime map is a system used to place varying steam injection behaviors into unique “bins” based on visual observations. The map indicates what behavior the steam condensation will have at various combinations of process conditions. Common process conditions used in maps include steam mass flux and water temperature. Regime names include various terms like “oscillatory bubble,” “condensation oscillation,” and “Oscillation-1” to describe the behavior of the steam jet.

Visual observations are used to describe the condensation due to the complex physics and large variety in behaviors that make quantitative comparison difficult. The qualitative nature of regime maps limits their usefulness, especially when the paper they are published in does not include good images of the described behaviors. Many papers use very similar terms like “oscillatory bubble” and “ellipsoidal oscillatory bubble” to differentiate regimes, but it is unclear what exactly these terms mean and how the behavior they describe is different. Additionally, the same regime name is often used to describe contradictory behavior in published papers by different research groups.

2.1.1. Regime Maps of Direct Contact Condensation in Quiescent Pools

Chan and Lee [4] presented one of the first regime maps to describe direct contact condensation. In their experiment steam was injected into a pool of water at atmospheric pressure and with “low” steam mass flux (0-175 kg/m^2-s). The map is defined by pool temperature and steam mass flux, both of which are commonly included parameters in most subsequent regime maps. Their rationale was that the steam mass flux provides a measure of the driving mechanism and the pool subcooling represents a measure of the condensation rate. The map published by Chan and Lee is shown in Figure 2-1.

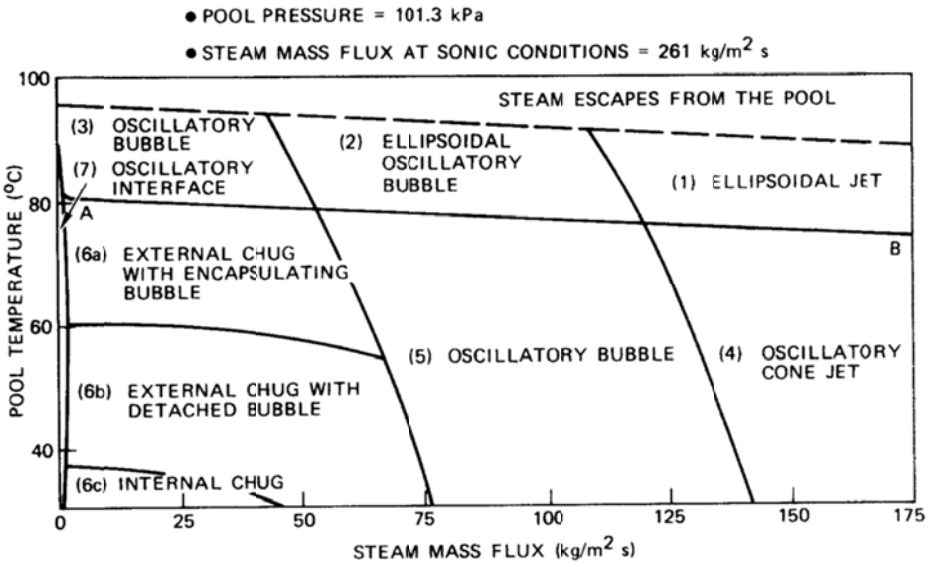

Figure 2-1. One of the first regime maps for steam injection from Chan and Lee

Chan and Lee summarized the regimes into categorizes based on “two criteria: (1) the location of the steam region relative to the pipe exit and (2) the location at which steam bubbles detach from the source.” This experiment used a nozzle with a 2 inch diameter oriented downwards into a pool of water. Bubble formation and separation was observed at 5-40 Hz.

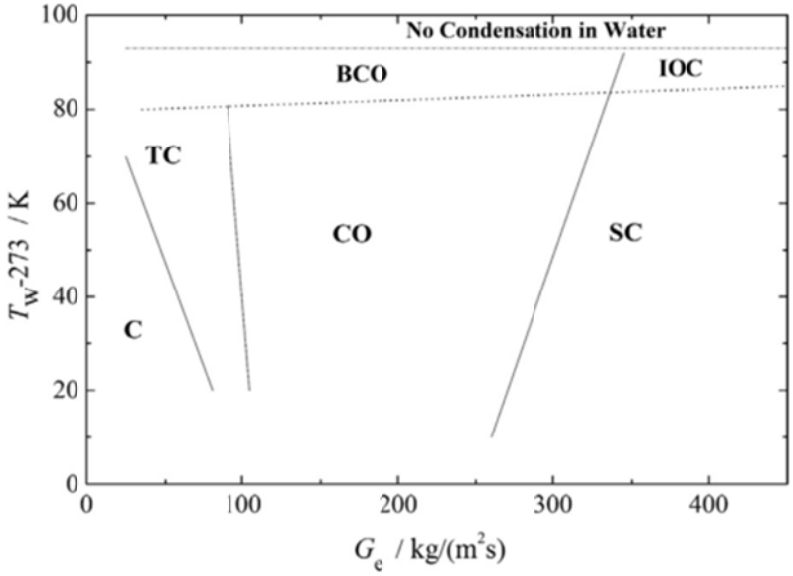

Figure 2-2. Regime map published by Cho et al. including further defined regimes.

Many other groups have developed their own regime maps and defined different condensation regimes. The regime map by Cho et al. shown in Figure 2-2 is referenced in most papers on direct contact condensation. Chugging (C) occurs at low steam mass flux and the liquid water is able to repeatedly enter the steam nozzle before the steam reemerges. Condensation oscillation (CO) is characterized by a violent oscillation of the steam and water interface. Bubbling condensation oscillation (BCO) includes the breakoff and collapse of steam bubbles from the main jet. Stable condensation (SC) occurs at high mass flux. Interfacial condensation oscillation (ICO) occurs at water temperatures when "the interface of the steam jet becomes unstable." It is not clear to the thesis author how ICO and CO differ.

Further efforts have been made to categorize regimes based on additional parameters including nozzle diameter, the difference between steam water temperatures,

and water sub-cooling. Petrovic de With et al. published the three-dimensional regime map shown below in Figure 2-3. This regime map splits the stable regime into more specific regimes including divergent jetting, ellipsoidal jetting, and conical jetting. This map doesn't indicate that nozzle diameter has a strong effect on regime transition behavior at low mass flux.

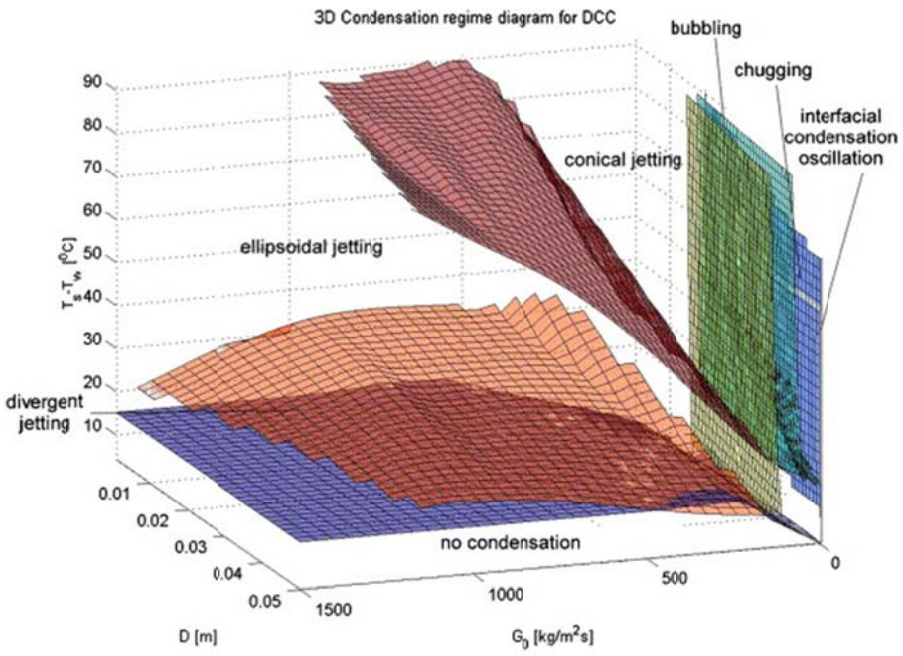

Figure 2-3 Regime map that includes varying nozzle diameter by Petrovic de With et al.

2.1.2. Regime Maps of Direct Contact Condensation in Flowing Liquid

Further complexity is introduced in regime maps when steam condensation in flowing water is considered and few examples were found in published literature. Recently (since 2010), research into steam injected into flowing water has increased. Studies mostly focus on steam injection concurrent with the water flow, but a few investigate injection into crossflowing water. However, the thesis author does not believe

that a full regime map using perpendicular steam injection into crossflowing water has been published. Only a map of stable condensation plume shapes was found [5].

Accounting for the effect of flowing water is usually considered by including the Reynolds number of the water flow as the 3rd parameter to define condensation regime. Figure 2-4 shows a regime map from steam injection concurrent with water flow in a pipe. In this map the chugging regime and stable regime are the same as described previously. The oscillation-1 regime and oscillation-2 regime descriptions are inconsistent and both seem to include behavior from the condensation oscillation regime and bubbling regime descriptions discussed previously.

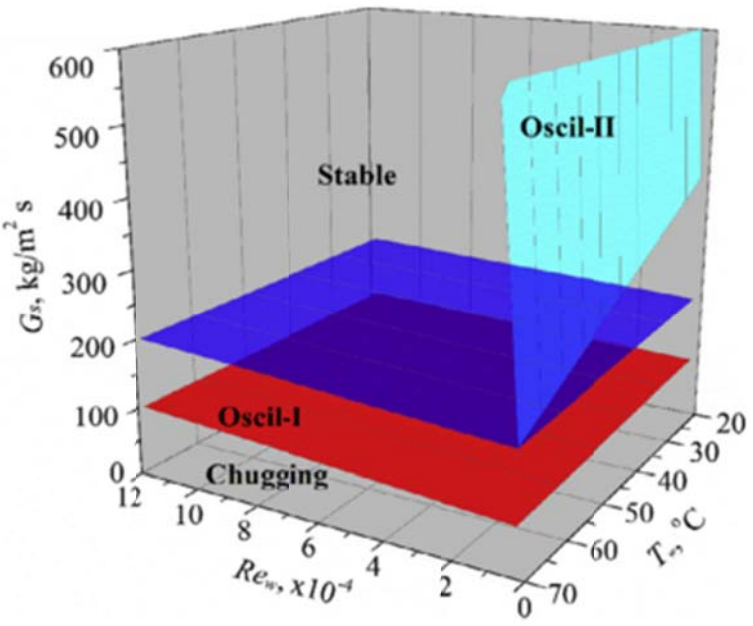

Figure 2-4. Regime map of behavior with steam injected concurrent to the water flow.

2.1.3. Summary of Regimes Discussed in Published Literature

Overall, regime descriptions in published literature are not always consistent and direct comparison is problematic. Minor variations in terminology are difficult to interpret due to the complex nature of the direct contact condensation behavior. However, four general condensation regimes are consistently present in the literature and will be used in this thesis:

(1) **Chugging:** This regime occurs at low mass flux when the steam plume is able to fully condense and water periodically enters the steam nozzle before the steam plume reemerges.

(2) **Condensation oscillation:** This regime occurs when a steam bubble is constantly seen at the nozzle exit and is continuously growing and shrinking while still attached to the nozzle exit.

(3) **Bubbling:** This regime is characterized by the growth and detachment of steam bubbles.

(4) **Stable condensation:** This regime is characterized by little variation in the steam plume volume. Stable condensation is sometimes split into more specific regimes based on jet plume shape.

2.2.Pressure Oscillation in Direct Contact Condensation

The audible noise produced by the steam injection at stable and unstable conditions is of particular interest to the research sponsor due to its negative effects on equipment operators. Additionally, the pressure fluctuations that produce the noise can cause process equipment damage. Simpson and Chan were among the first to investigate

the pressure oscillations created by the steam injection [6]. Simpson and Chan included discussion on five trends seen in their experiment:

1. Pressure oscillation frequency increases with increasing pool subcooling.
2. Pressure oscillation frequency decreases with increasing injection tube diameter.
3. Pressure oscillation amplitude increases with decreasing pool subcooling
4. Pressure oscillation amplitude increases with increasing injection tube diameter
5. Increasing pressure amplitude with increasing exit mass flux

These general trends are confirmed in nearly all subsequent studies on direct contact condensation. Nariai and Aya clarified that the pressure oscillations have the same frequency as the movement of the steam and water interface through the use of visual observation, but the behavior could not be proven quantitatively due to the testing equipment available [7]. Modern high speed cameras and pressure measurement devices allow for the pressure oscillation signals of the condensation regimes to be analyzed in detail.

2.2.1. Pressure Oscillation in the Condensation Oscillation Regime

Figure 2-5 shows a series of images of a steam plume in the condensation oscillation regime. The plume is shown to alternately grow and contract and bubble-like shapes are formed, but do not separate from the main plume. This volume change

induces a pressure fluctuation in the water of similar relative magnitude and is shown in Figure 2-6.

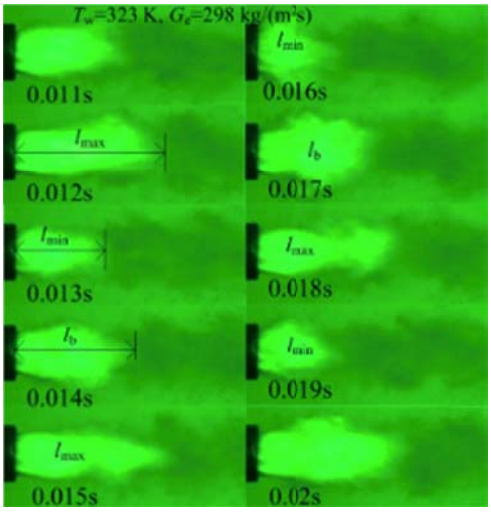

Figure 2-5. Images showing a steam plume in the condensation oscillation regime from Qiu et al. [8].

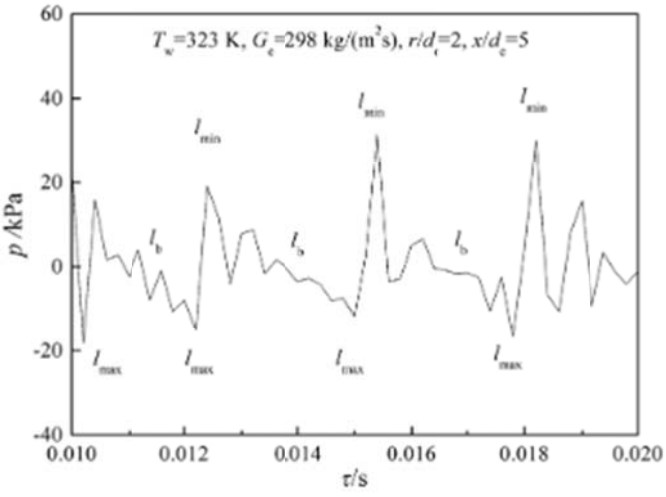

Figure 2-6. Pressure oscillations caused by the plume volume change shown in Figure 2-5 [8]**.**

2.2.2. Pressure Oscillation in the Bubbling Regime

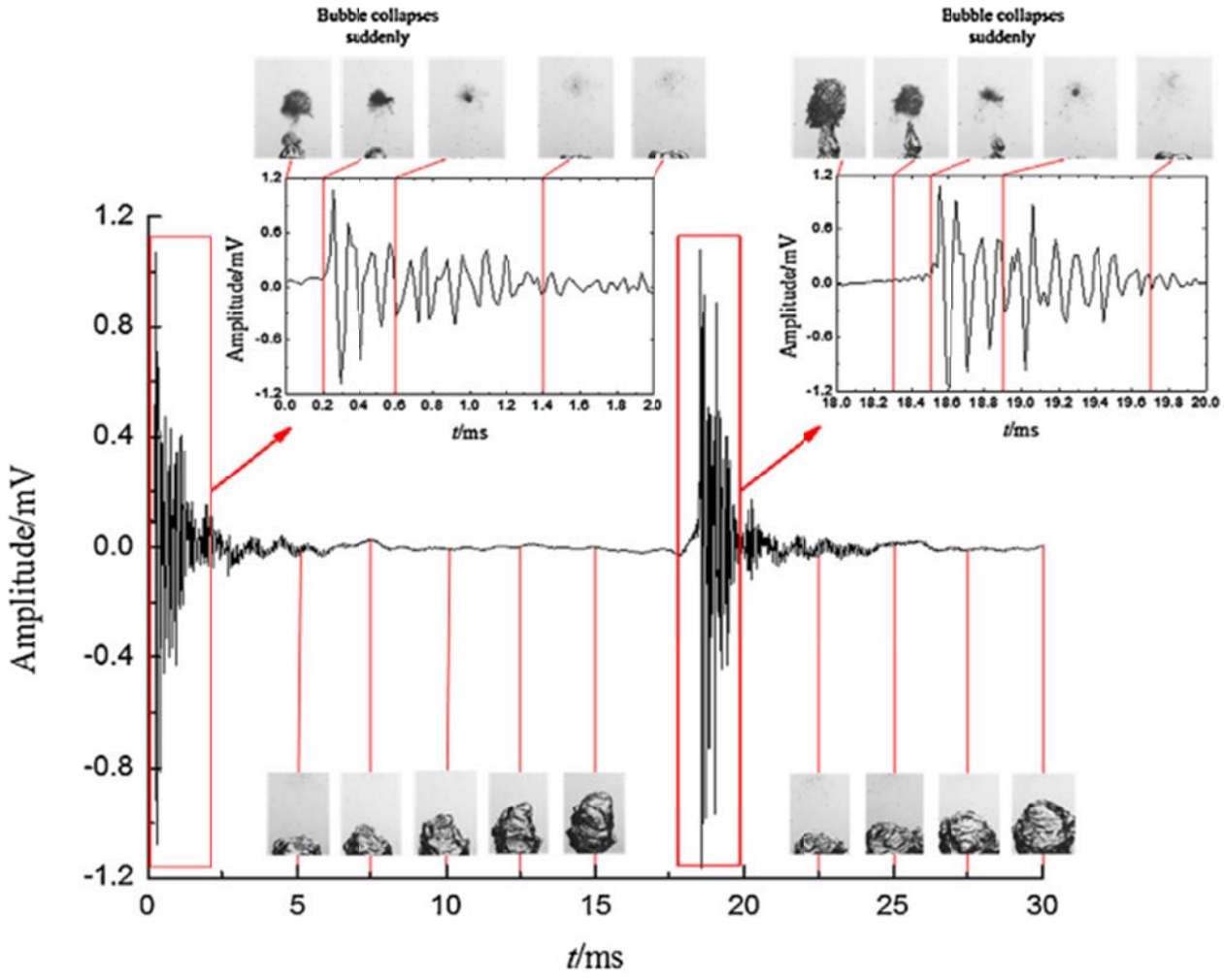

Figure 2-7. Comparison between acoustic signal and bubble collapse images from Tang et al. [9]

Pressure oscillation of the plume in the bubbling regime is caused by the collapse of steam bubbles that break off from the main steam jet. This behavior is shown using a combination of visual images and acoustic signal data from Tang et al. in Figure 2-7. The link between plume volume oscillation and water pressure fluctuation is a key behavior exploited in this thesis.

3. Experimental Setup

3.1. Equipment Description

3.1.1. Overview of Test Facility

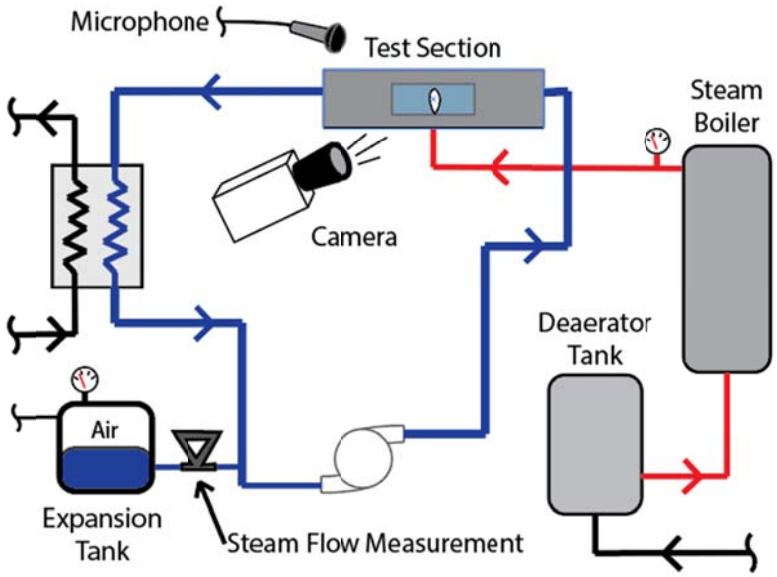

Figure 3-1. Test skid schematic showing the major components.

A schematic of the test skid is shown in Figure 3-1 and a picture of the skid is shown in Figure 3-2. During start up, saturated steam is produced in the steam generator and is used to heat the water in the deaerator tank. Once the deaerator tank is heated, the deaerated water is pumped into the process water loop. Water is pumped around the process water loop using a single speed centrifugal pump and flow rate is manually controlled using a recirculation loop and flow restriction valve. During normal operation, the steam is injected into the process water loop in the test section. The steam temperature set-point is maintained using resistive heating wire installed on the outer surface of the steam lines. The steam mass flow rate is measured by a Coriolis flow

meter measuring the flow of liquid water into the expansion tank; at steady state this mass flow of liquid water out of the loop must equal the mass flow of steam into the loop. The expansion tank maintains and controls the loop pressure. The cooling water loop uses a chilled water supply to control the temperature of the process water loop using a heat exchanger. Details of each major component are included in the following sections.

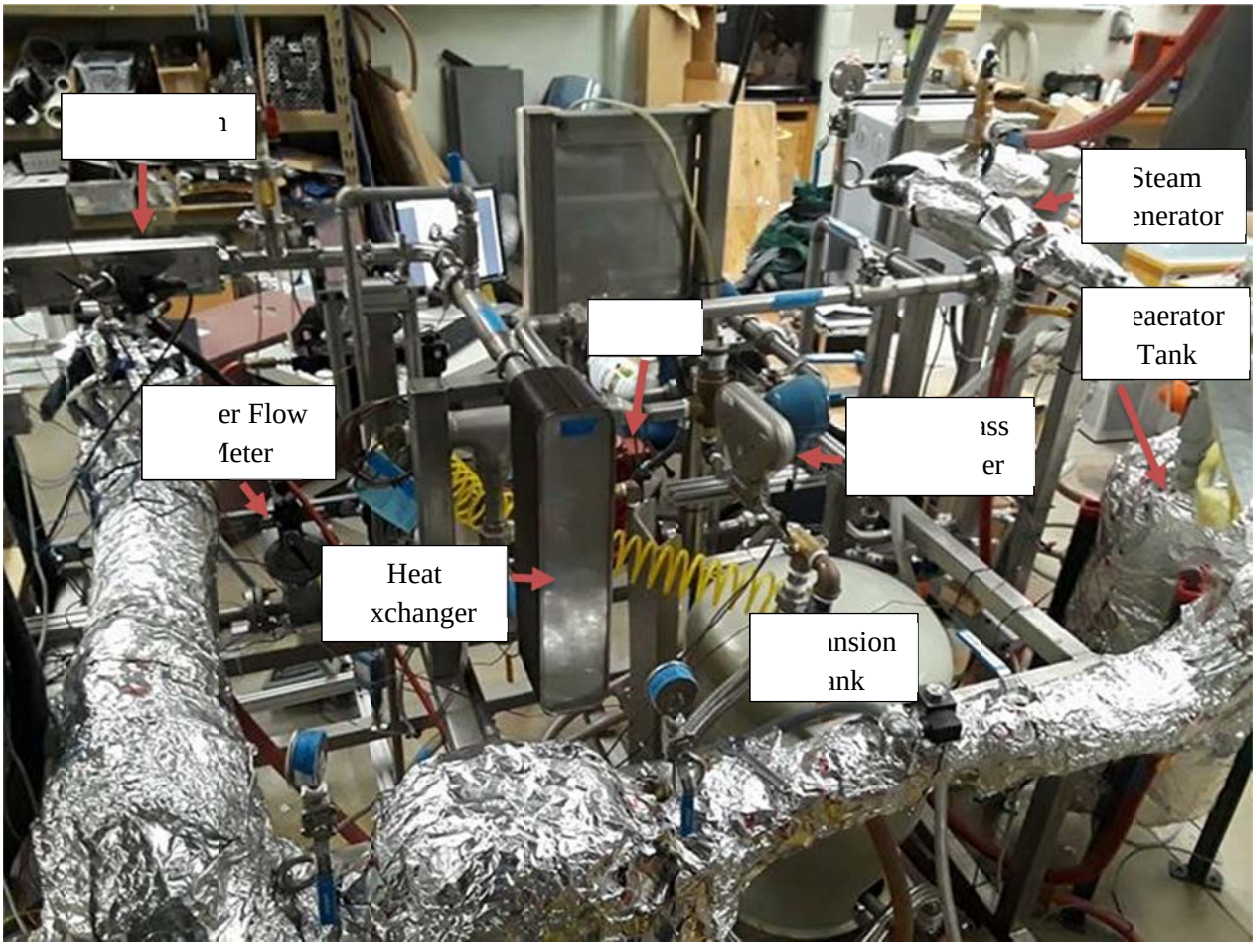

Figure 3-2. Picture of the test skid showing major components from the schematic diagram.

3.1.2. Steam Generator

An Infinity Fluids 480 V, 48 kW electric boiler is used as the saturated steam source. The temperature is controlled by a PID temperature controller interfaced to a K type thermocouple and is accurate to +/- 1 degree Celsius. This equates to an accuracy of about +/- 2.5 psi at the high end of the steam pressure range. A liquid over-pressure safety valve opens to drain at 100 psig. Due to pressure fluctuations about the set-point, the steam generator can produce steam up to about 95 psig. The steam generator also has an emergency blow off valve at the vapor outlet which opens at 125 psig and exhausts steam through a hose attached to the drain stack. The feeder pump automatically controls liquid level in the steam generator body using a float switch. An override switch was installed to allow the pump to be turned on manually to fill the test section loop with deaerated water from the deaerator tank prior to testing. A set of valves was installed to switch the pump outlet flow for this purpose. The yellow handled ball valves shown in Figure 3-3 switch the flow and the red handled gate valve allows for controlling pressure output of the feeder pump when filling the process water loop.

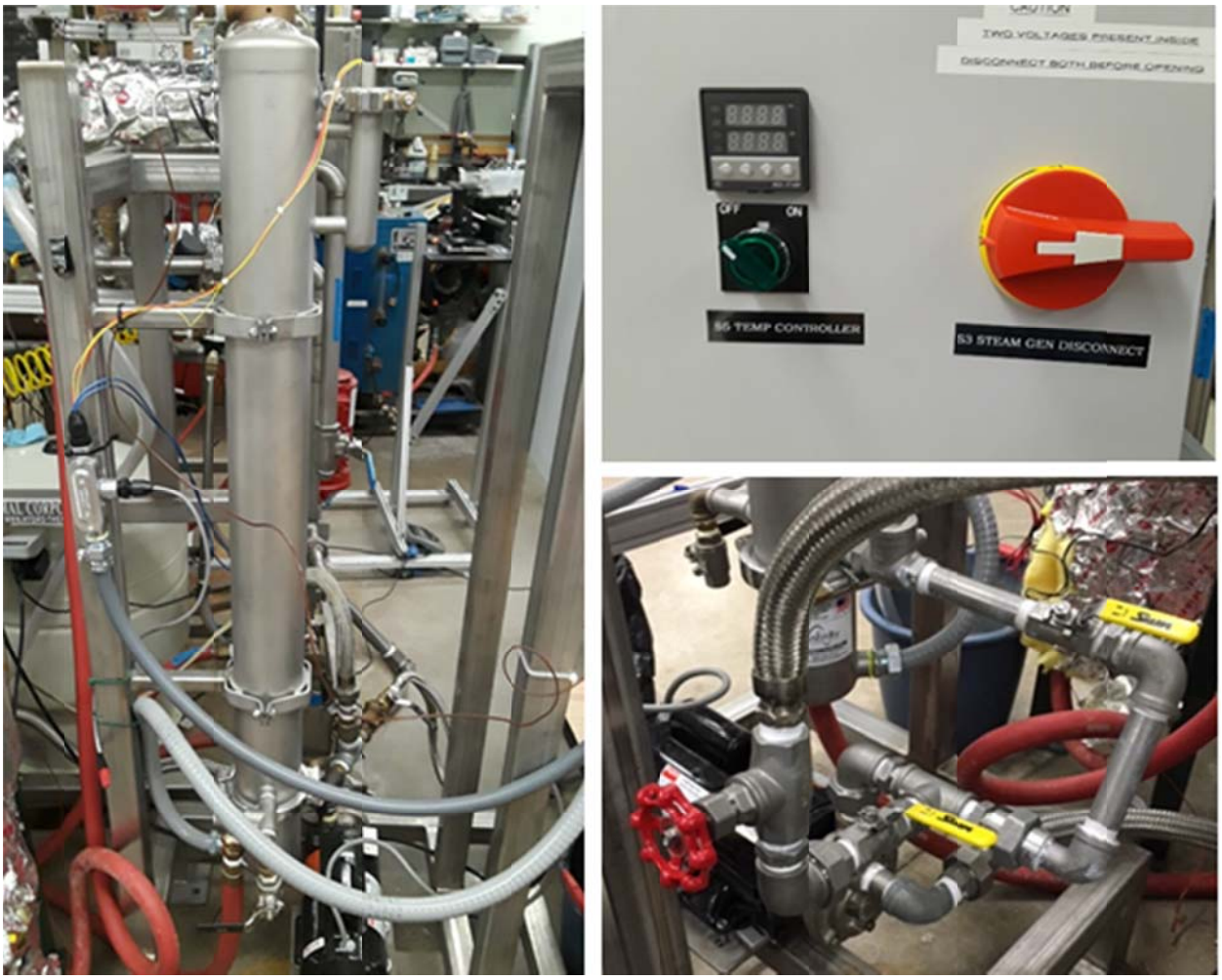

Figure 3-3. Steam generator, temperature controls, and boiler pump outlet flow control.

3.1.3. Insulation and Additional Steam Heating

Insulation is used on all of the steam lines to prevent the steam from condensing. Steam line insulation is mostly fiberglass wrap covered in aluminum foil and secured with foil tape. Additionally, the approximately 5 feet of steam lines leading into the test section are wrapped with 1.2 kW of resistive heating wire. The insulation on this portion of the steam piping is mineral wool due to the high temperature of the heating wire, which damaged the fiberglass insulation previously used on that section. The heating

wire power input is controlled by a PID temperature controller interfaced with a thermocouple touching the exterior of the steam piping and heating wire. A thermocouple measuring steam temperature directly was used initially, but the lag time between heat input and changing steam temperature was too great to be controllable. The current strategy is to set the heating wire PID controller to approximately 30 ˚C above the desired steam temperature.

The resistive heating wire and a small amount of steam throttling allow for the steam to be superheated by several degrees Celsius. A small amount of steam superheat ensures that 100% vapor steam is being injected and allows for the determination of inlet steam specific enthalpy using the measured temperature and pressure. The specific enthalpy is subsequently used in an energy balance to calculate the rate of input steam mass. This energy balance was used to validate the condensate steam mass flow method mentioned in a later section. In the future, combining the energy balance method and condensate steam mass flow method could be used to test the effect of low quality steam on condensation stability.

3.1.4. Steam Pressure and Temperature Measurement

The produced steam temperature is set using the steam generator, which in turn sets the steam pressure since the generator produces saturated steam. The steam pressure is measured just before the test section input using a Baumer high temperature pressure transmitter. The pressure transmitter has a range of 0-230 psi and accuracy of +/-0.25% of the full scale. The steam temperature was also measured using a type K thermocouple which has an uncertainty of +/-2.2 C.

3.1.5. Steam Mass Flow Measurement

The steam mass flow is determined by measuring the mass flow rate of liquid water entering the expansion tank. The steam mass flow measurement exploits the incompressibility of water to measure steam mass flow. A plot of process water loop pressure with time with a normal steam injection rate of 4.5 [g/s] and the expansion tank disconnected is shown in Figure 3-4. The process water loop has a volume of approximately 2 gallons.

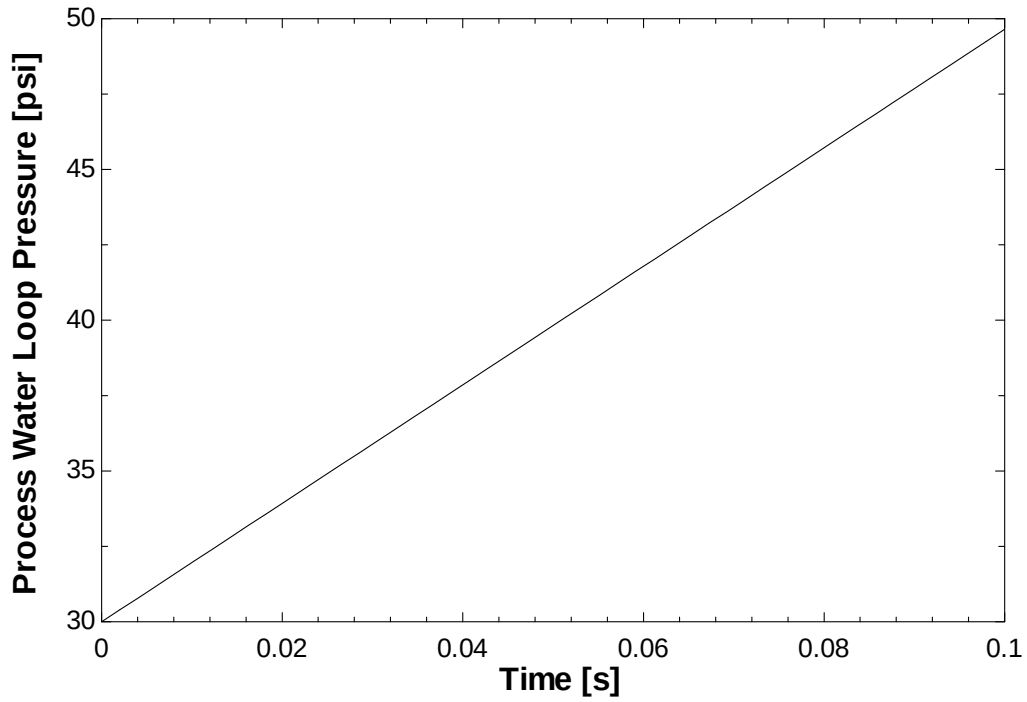

Figure 3-4. Sealed process water loop pressure over time with a 4.5 [g/s] steam injection rate.

Figure 3-4 indicates that if the expansion tank were disconnected, with steam being injected, the process water loop pressure would increase at a theoretical rate of approximately 200 [psi/s]. However, with the expansion tank connected, process water

loop pressure is maintained at a constant value over time. This indicates that the mass of water in the process loop volume must be constant, at least on an average basis, and therefore water mass that leaves the loop and enters the expansion tank must balance with the mass of water entering the loop as steam. An Emerson micro-motion Coriolis type meter used to measure liquid water flowing into the expansion tank. It is a model CMF010M and is shown in Figure 3-5. The steam mass flow meter has an accuracy of 0.1% of the measured value.

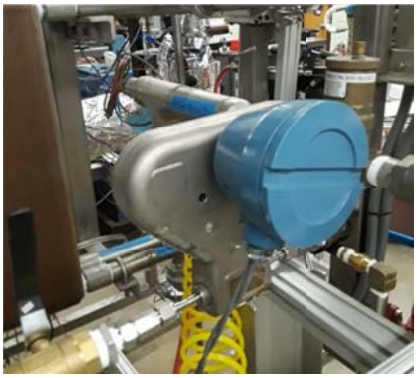

Figure 3-5. Steam mass flow meter.

The steam mass flow measurement technique was further validated using an energy balance method. The temperature, pressure, and flow rate of the steam and water were measured entering and exiting the test section. For this test an entering water temperature of 30 [˚C] and 12 [gal/min] was used along with water and steam pressure of 30 [psig] and 82 [psig], respectively. The test section and process water pipe between temperature measurement points was also insulated extensively. Results of this study are shown below in Table 1. Note that the temperature rise across the test section was

recorded with no steam injection and this correction was added to account for minor differences in the thermocouples (0.085 ˚C).

Table 1. Steam Mass Flow Method Validation Study

Run Number	Mass Flow from Energy Balance [g/s]	Liquid Steam Mass Flow Method [g/s]	Percent Difference [%]
1	1.271	1.228	3.441
2	1.261	1.226	2.815
3	1.254	1.246	0.64
4	1.251	1.238	1.045
5	1.252	1.242	0.802

As Table 1 indicates, the maximum percent difference was 3.44% and the average was 1.75%. The difference is likely due to the use of seven measured variables in the energy balance method. The values are similar enough to move forward with the liquid steam mass flow method.

3.1.6. Deaerator Tank

A deaerator tank is used to remove air from the water in the tank by heating it. The deaerated water is used to feed the steam generator and is also used to fill the test section loop prior to beginning a testing session. The deaerator tank has a temperature controlled thermostatic valve which maintains the deaerator temperature at approximately 92 [˚C] by sparging in steam. Holding the water temperature at 92 [˚C] should decrease the dissolved oxygen by at least 90%. The solubility of oxygen in water as a function of temperature provided by engineeringtoolbox.com is shown in Figure 3-6.

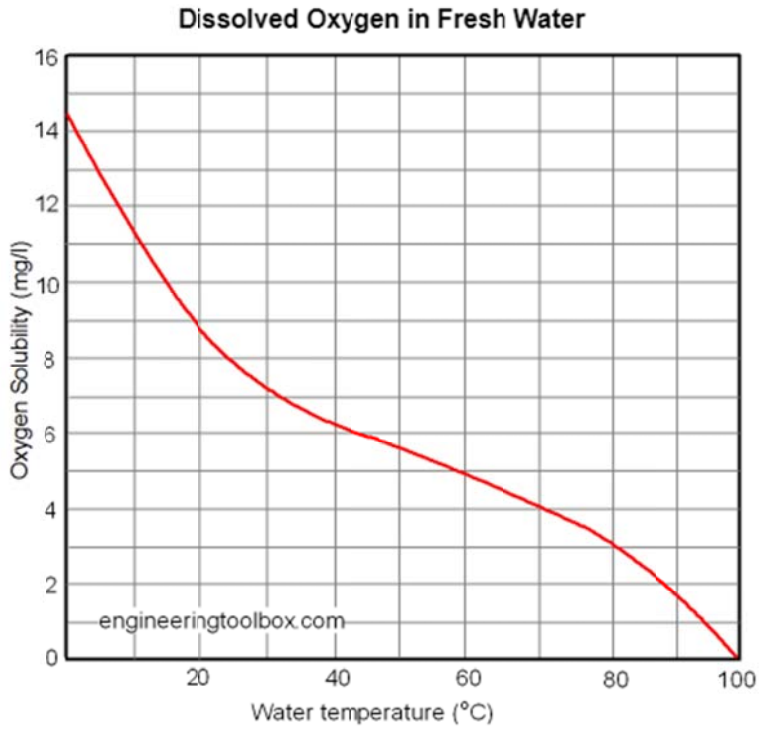

Figure 3-6. Dissolved oxygen in water as a function of temperature at atmospheric pressure.

Using deaerated water is important for several reasons. First, oxygen in the steam contributes to corrosion of the steam piping and associated components. Second, gasses in the liquid process loop water obscure the high speed videos and interrupt data processing. Third, other published literature and qualitative observations from Hydro-Thermal Corporation indicate that air in the process water affects condensation stability and noise. The deaerator tank, solenoid fill valve, and thermostatic temperature control valve are shown in Figure 3-7.

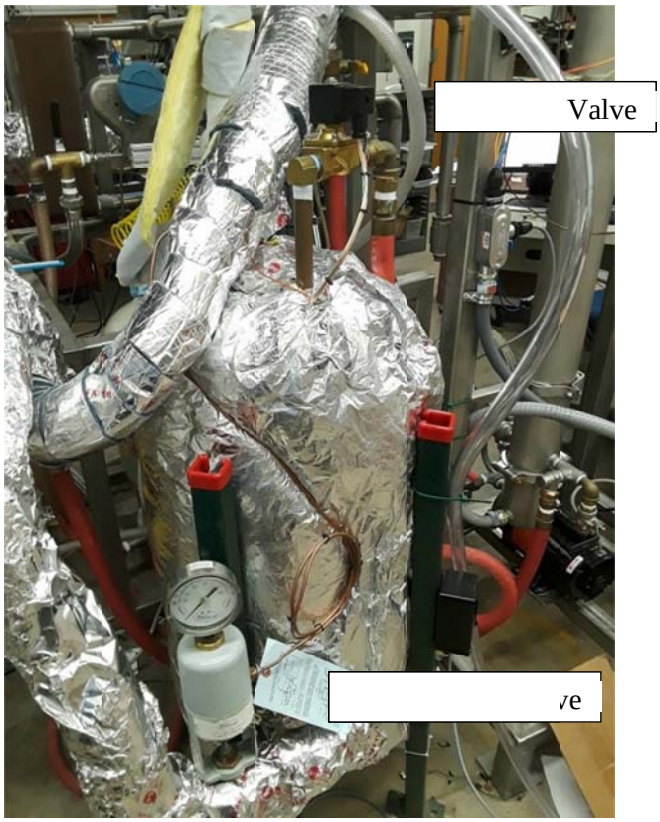

Figure 3-7. The deaerator tank and associated control components.

Filling of the deaerator tank is controlled using the solenoid valve indicated above. An Arduino running a simple program monitors a float switch and sends a signal to the solenoid to hold open for 4 seconds to input water into the tank. The valve opens for 4 seconds to prevent waves in the tank from quickly triggering the solenoid on and off and creating a "chattering," which previously created leakage issues due to frequent water hammering in the supply pipes.

3.1.7. Expansion Tank and Water Pressure Measurement

An Amtrol Therm-X-Trol ST-60V hydronic expansion tank is used to control the process water pressure. A pressure regulator controls the air pressure in the expansion

tank and thus controls the process water pressure through a rubber bladder interface similar to the schematic shown in Figure 3-8. As steam is injected into the process water loop the expansion tank accepts an equal amount of water to keep a constant pressure in the process water loop. The tank has a 34 gallon capacity which allows the experiment to run for several hours at normal steam mass flow rates before the tank needs to be emptied. The expansion tank is on a digital scale, which allows for the tank fill amount to be calculated. The change in weight over time was used to further validate the mass flow value output by the Coriolis liquid steam mass flow meter.

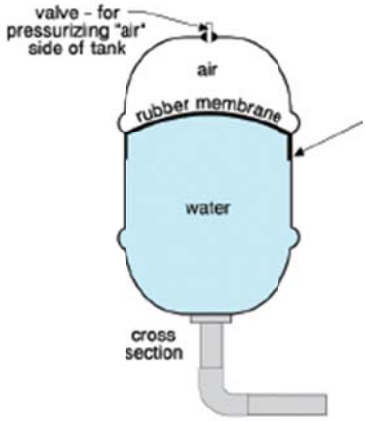

Figure 3-8. Cross Section of Typical Expansion Tank from ASHI Reporter.

Water pressure at the steam injection point was originally measured using an Omegadyne PX209-100A5V pressure transducer. Partway through testing this pressure transducer started to malfunction. This may have been caused by repeated exposure to the high frequency pressure fluctuations produced by unstable condensation. The pressure transducer was replaced by an SSI Technologies P51-100-G with an accuracy of +/- 1% of full scale partway through the testing in this thesis.

3.1.8. Centrifugal Water Pump and Water Flow Measurement

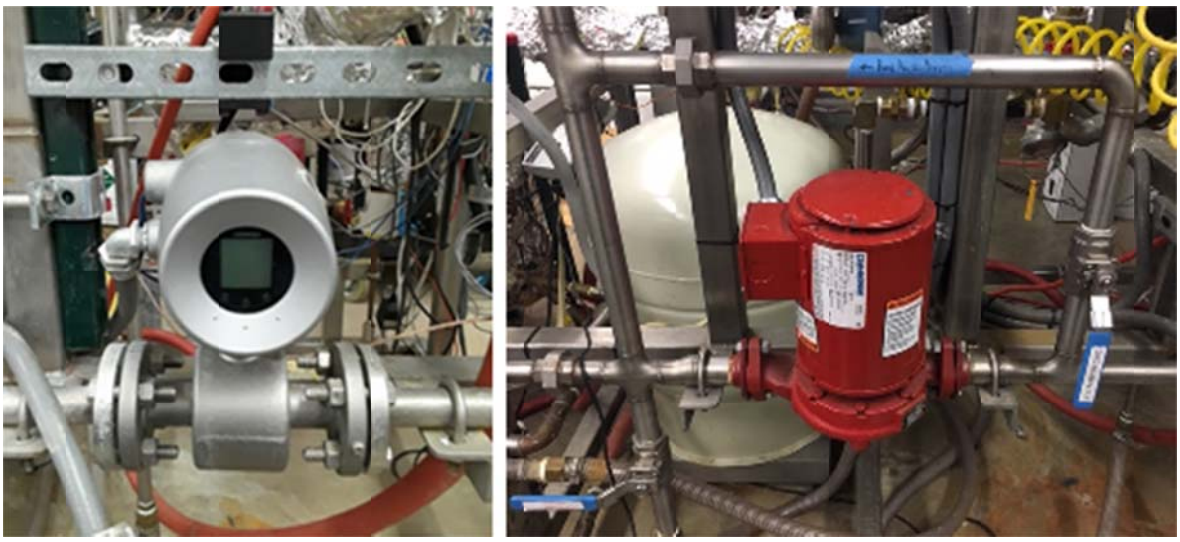

Figure 3-9. The water flow meter (left) and centrifugal pump with recirculation loop (right).

A Bell & Gosset 90-4T centrifugal pump rated for high temperature is used to pump the test section loop water. The pump can produce a water flow rate up to 20 [gal/min]. The pump is single speed and flow rate is manually controlled using a restriction valve and pump bypass recirculation loop. A Toshiba GF630 electromagnetic flow meter is used for measuring the water flow. The flow meter has a range up to 75 [gal/min] and is accurate to +/- 0.2% of the flow. The lining of the water flow meter is the limiting factor that leads to a maximum water loop temperature of approximately 93 [˚C].

Figure 3-10. Heat exchanger for cooling water loop (left) and cooling water flow meter (right).

3.1.9. Process Water Temperature Measurement and Control

The test section water temperature was controlled using a heat exchanger interfaced with a cooling water supply. The cooling water flow rate was controlled using a gate valve, which in turn controlled the temperature of the test section water. The valve was manually controlled and was opened or closed until the desired temperature was reached. A simple analog flow meter was installed to provide a general indication of the water flow rate when making small adjustments. The temperature of the cooling water flow was about 15 [˚C], which limited loop temperature to a minimum of approximately 20 [˚C]. Heating of the process water was accomplished inherently due to the steam injection process. Two type E Thermocouples with an uncertainty of +/-1.7 C were used to measure the temperature of the water at the inlet and outlet of the test section. This data was read into LabVIEW using the data acquisition system.

3.2. Data Acquisition System

A National Instruments cDAQ-9178 platform is used to record all of the experimental data. Table 2 indicates the measurement type, cDAQ card, and sampling rate for each data type.

Table 2. cDAQ cards used and their sampling rates

Data Type	Measurement Type	cDAQ Card	Sampling Rate
Pressure Transducers	Voltage and Current	NI 9207	1 kHz
Thermocouple temperatures	Voltage	NI 9211	1 kHz
Camera trigger and microphone signal	Voltage	NI 9215	100 kHz

3.2.1. High Speed Camera

The high speed video images presented in this thesis were taken using a Phantom V311 camera. The camera is capable of up to 3 billion [pixel/second] output. This equates to 3250 fps at 1280 x 800 resolution. Faster frame rates can be achieved at lower image resolution. Most high speed video data presented in this thesis was taken at 81,000 fps and 128 x 200 resolution. This frame rate was chosen in order to capture approximately 10 images per cycle of the highest frequency steam plume oscillation discussed in a later section. The resolution allowed was then dictated by the camera's pixel throughput limit. At 81,000 fps the exposure time for each image was 11.642 microseconds. The camera trigger signal was measured by the data acquisition system which then automatically saved microphone data in sync with the camera images. This feature was not used in this thesis, but would be useful in the future to sync high speed pressure measurement with camera images.

The Phantom V311 was equipped with a Nikon Micro-Nikkor 55mm macro lens. Several different lenses were experimented with and it was found that the Micro-Nikkor lens provided the best images qualitatively. Lighting of the steam plume was accomplished using a Dolan-Jenner MI-150 Fiber-Lite. The best images were captured when the overhead lab lights were turned off, a cardboard box was placed over the test section and camera to block incident light, and the fiber-lite was aimed at the steam plume such that extra light not reflected off of the plume passed through the rear window of the test section.

3.2.2. Microphone

Audio data presented in this thesis was recorded using an Audio-technica AT3527 microphone and Symetrix 302 Dual Microphone Preamplifier.

3.3. Visualization Test Section

The work presented in this thesis required a redesign of the previously existing visualization test section. The original test section used large windows made of acrylic. This design was meant to visualize the steam being injected into the water as well as the jet of hot water created by the steam as it mixed with the water. The large window had relatively low pressure and temperature limits due to its size and the material properties of acrylic. The test section also leaked constantly due to its odd sealing interfaces. New specifications were developed along with Hydro-Thermal and a new test section was designed capable of continuous 100 [˚C] temperature exposure and 100 [psig] internal pressure. The new test section is shown in Figure 3-11.

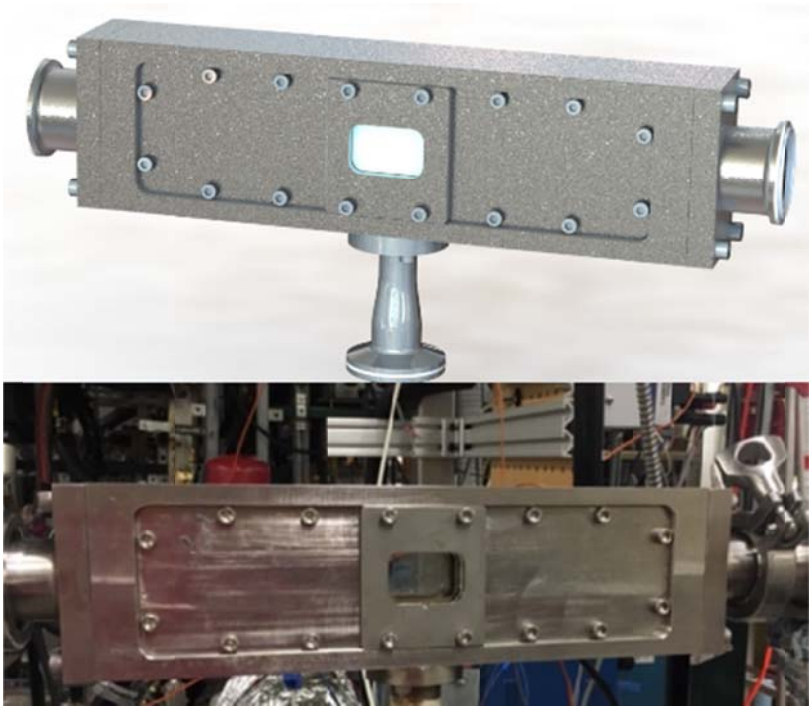

Figure 3-11. Visualization test section rendering (above) and installed picture (below).

The main body and most of the components of the test visualization section are made from type 316 stainless steel for strength and corrosion resistance. Hydro-Thermal Corporation manufactured the test section at their facility. Special thanks to Fred Kottke for his advice during design of the test section and work producing manufacturing documentation.

The visualization test section was designed to accept brass nozzle plugs in the steam entrance in a similar fashion to the previously used visualization test section. The brass plugs allow for easy machining and installation of a nozzles with varying diameter, length, and entrance geometry. An example of a nozzle plug is shown on the left in Figure 3-12.

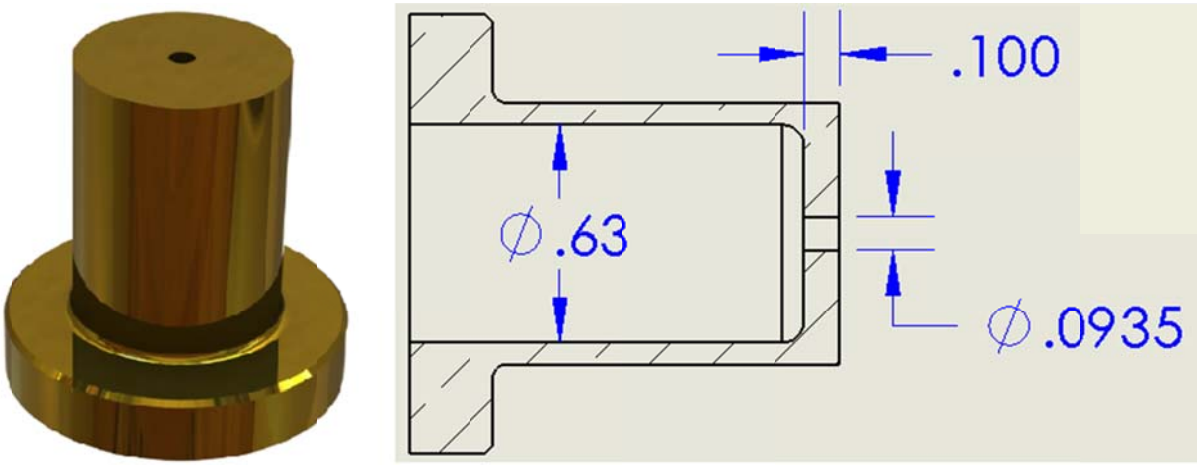

Figure 3-12. Example nozzle plug (left) and example nozzle plug dimensions (right, dimensions are in inches).

Figure 3-12 also shows example nozzle plug dimensions on the right. All nozzles tested for this thesis were straight-bore orifices. The dimension indicated as 0.100” is the length of the nozzle, the dimension indicated as 0.0935” is the nozzle diameter, and the dimension indicated as 0.63” is the diameter of the steam section upstream of the nozzle.

The visualization test section includes a window on the front and back of the section to allow optical access for high speed video recording. The window on the rear of the section allows light not reflected off of the steam plume to pass through and not degrade image quality by being reflected off of the inner test section walls. Fused quartz was chosen as the material for the viewing windows due to its high strength and low coefficient of thermal expansion. The window was required to be manufactured with a flange to meet requirements of test section water flow area and to allow for the nozzle plug entrance diameter to be large relative to the nozzle size. Technical Glass Products in Ohio was chosen to manufacture the windows because it was the cheapest option.

4. Data Processing and Analysis Methods

Three types of data were collected for each experimental test condition or “data point” in order to characterize the steam condensation behavior: Process conditions (temperatures and pressures), high speed video, and audio data.

4.1. Process Parameter Measurements

Process temperatures, pressures, and flow rates were measured continuously to ensure safe conditions while the test facility was operating. For the testing described in subsequent sections nominal values for desired process conditions were prescribed as part of the test plan. Actual, measured process conditions varied slightly from the nominal, prescribed values. For each data point, the 30 seconds of process condition data proceeding the high speed video capture were saved to verify that the condition was roughly steady state and to accurately characterize the data point conditions. A data point was considered to be sufficiently close to the prescribed condition and at steady state if the water temperature recorded was within +/- 0.5 [˚C] of the desired temperature for the 30 seconds prior to the high speed video capture. An example of measured temperature data is shown in Figure 4-1.

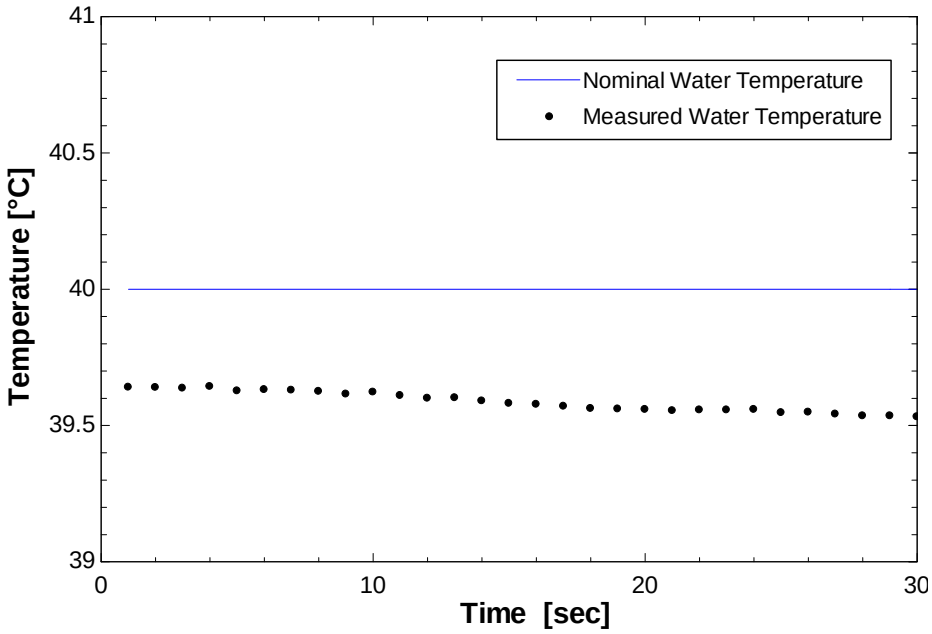

Figure 4-1. Example measured water temperature data that meets the steady state condition requirement.

Water temperature was chosen to determine whether a point was steady state because it was the parameter that was most difficult to control and was also the input that was varied most frequently during the testing. Steam pressure was automatically controlled by the steam generator PID controller. Water pressure was initially set manually and then was held at a relatively constant value by the air pressure regulator connected to the expansion tank. Water temperature and water flow rate were the two process variables with true manual control. Water flow rate stayed essentially constant after being initially set by manually operating the flow restriction valve (due to the relatively constant water pressure). However, water temperature needed to be actively monitored during testing and cooling water flow rate varied frequently. Through experience, the best method to control process water temperature was to slowly move between temperature data points by modulating the cooling water such that water temperature increased at a slow, steady

rate over time. This allowed for time to save high speed video recordings (~8 minutes) between each data point. Making large adjustments to the cooling water flow rate often caused overshooting of the desired temperature.

4.2.High Speed Video Acquisition and Analysis

4.2.1. High Speed Camera Output

A Phantom V311 camera described in an earlier section was used to record high speed video for analysis. The camera natively outputs .cine files, which is the Phantom proprietary file type and includes detailed information about the time of video capture, frame rate, exposure time, etc. At the 81,000 Hz framerate and 128 x 200 resolution the camera could only record about 2.1 seconds of video on the built in RAM. It was determined that 1 second of recorded data was sufficient to represent each data point and reduce the time required to save each file during testing. At the 81,000 framerate even the fastest plume oscillations (~8 kHz) were captured thousands of times. Each .cine file was about 4 GB in size for 1 second of video and required about 8 minutes to save. One circumstance where more data would have been useful is in the flip-flop regime discussed in a later section. This regime was characterized by two distinct behaviors that alternated back and forth quickly, but with a time scale that was similar to the 1 second recording time. A longer data set would be valuable for understanding the frequency of oscillation for each behavior and the amount of time the plume spent exhibiting each behavior.

It is recommended that in the future a solid state hard drive be purchased to allow more rapid transfer of recorded videos so that longer video recordings can be saved in a

reasonable amount of time. The solid state hard drive would act as a temporary and intermediate storage device for each testing session before the files are transferred to a larger and more economical disk drive overnight. The solid state hard dive would also make the next step in the process much faster, conversion of .cine files to .tiff.

4.2.2. High Speed Video File Conversion

Phantom .cine files can only be opened in the Phantom software. Before the high speed videos can be analyzed in MATLAB they need to be converted into individual .tiff files. Multipage .tiff files are more convenient to work with, but due to the size of the multipage .tiff files (4 GB) computer RAM space was a concern when manipulating the images. Phantom CV software was used to perform the conversion to .tiff files, which took approximately 20 minutes for each 1 second of video. The conversion was initially done in the background while performing other tasks. However, the file conversion time became a significant factor when the volume of data being collected increased towards the end of the project. The Phantom software batch convert function was then utilized to process file conversion overnight.

4.2.3. Image Files in MATLAB

The individual .tiff files are imported into MATLAB and manipulated using the image processing toolbox. A .tiff image is imported into MATLAB and represented as an array of intensity values. Since the Phantom V311 records in greyscale, the intensity value of each pixel represents the degree of greyness of that pixel. Images are saved as 16-bit .tiff files so each pixel has a possible value of 0 to 65,535 with 0 representing completely black and 65,535 representing completely white. Figure 4-2 shows an

example image on the left and a zoomed in portion on the right showing the intensity values.

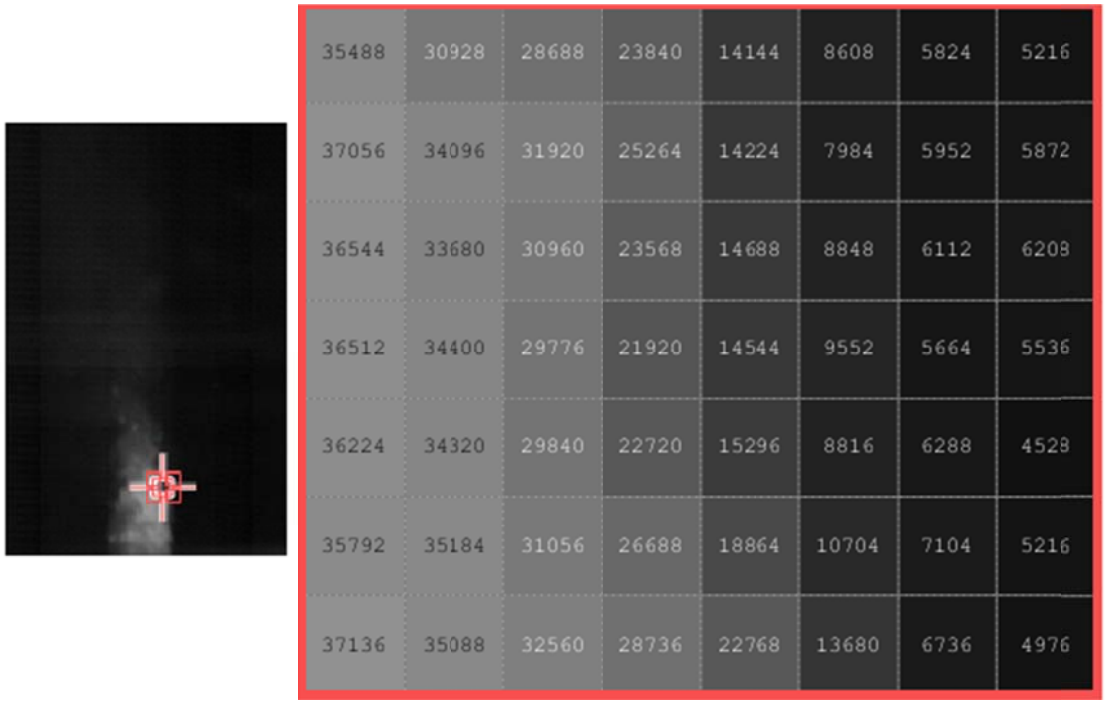

Figure 4-2. Example steam plume image with magnified region showing intensity values.

The intensity values shown in Figure 4-2 illustrate the distinct difference between the pixels showing complete water (to the right in the magnified region ~5000) and the pixels showing complete steam (to the left in the magnified region ~36000). The example image and intensity values help to illustrate two key problems that occur when trying to quantitatively interpret the high speed images: (1) absolute intensity values are arbitrary and (2) the pixels that represent the steam plume edges are non-distinct and the edge location is difficult to define with certainty.

Absolute intensity values are arbitrary because the intensity is dependent on the lighting setup, how clean the test section windows are, how the steam plume shape

reflects light, and many other factors. For this reason it is difficult to directly compare images from videos that are taken on different days. These factors also make it difficult to objectively define the steam plume edge. The definition of the steam plume edge is important for the plume volume oscillation magnitude and frequency determination discussed in a later section. A plot of the pixel intensity vs. horizontal spatial location is shown in Figure 4-3 for the bottom three rows of the magnified region in Figure 4-2.

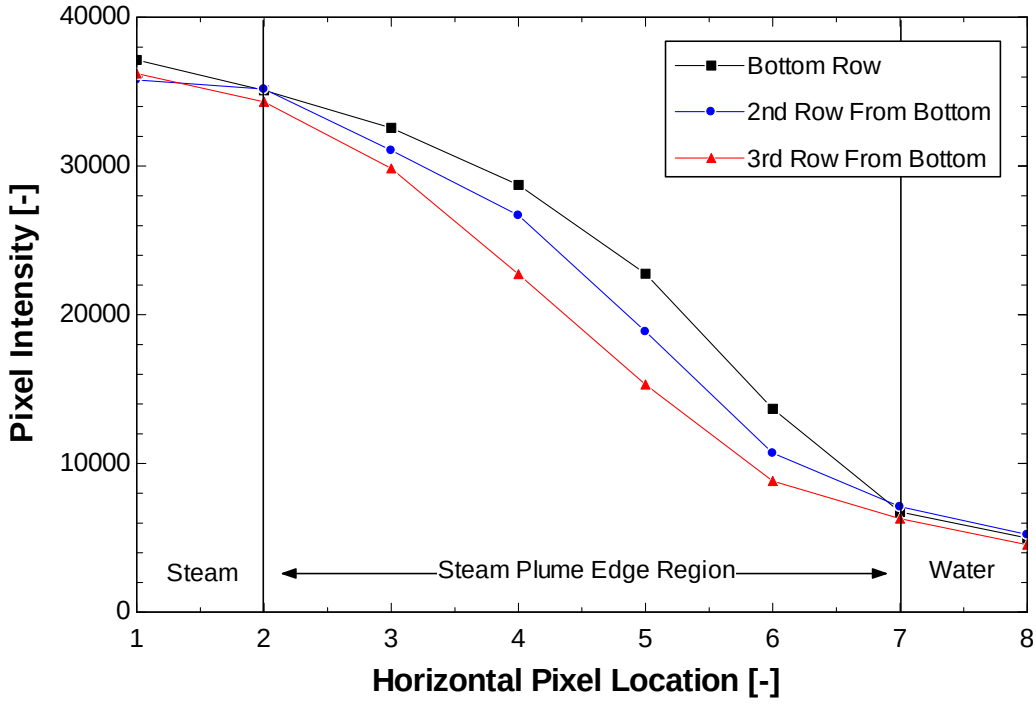

Figure 4-3. Plot of pixel intensity vs. horizontal location for the bottom rows of pixels shown in Figure 4-2.

The previous figure shows the intensity value as a function of horizontal pixel location. The region on the left (i.e., pixels 1-2) has a small derivative and is distinctly steam while the region on the right (i.e., pixels 7-8) has a small derivative and is distinctly water. However, the steam plume edge region (i.e., pixels 2-7) has a relatively

larger and changing derivative. Arguments could be made for defining the plume edge at pixel location 2, pixel location 7, or somewhere in between, such as the position where the derivative of the intensity function is the largest. In this thesis the steam area is defined using an intensity filter for simplicity (discussed in the subsequent section). A future area of improvement is to utilize a more robust edge finding method such as defining the point of most positive and most negative derivative as the left and right plume edges, respectively.

4.2.4. Image Intensity Filtering

In order to extract data about the oscillation of the steam plume volume, a quantitative distinction must be made between the steam plume and surrounding water. One of the most basic methods used to do this is with an intensity filter. An intensity filter converts the array of intensity values representing the greyscale image into an array of binary values using a simple greater than logical expression.

$$If\ Pixel(x,y) \geq Threshold\ Value, \qquad Pixel(x,y) = 1$$

Pixels with an intensity greater than or equal to the threshold value are given a binary value of 1 (steam) and pixels with an intensity of less than the threshold value are given a binary value of 0 (water). Determination of the threshold value is subjective. The same value cannot be used for all videos, especially from different testing days, due to the lighting factors discussed earlier. The influence of the threshold value choice on the results is discussed in a later section. The binary image resulting from the use of an intensity filter is shown in Figure 4-4.

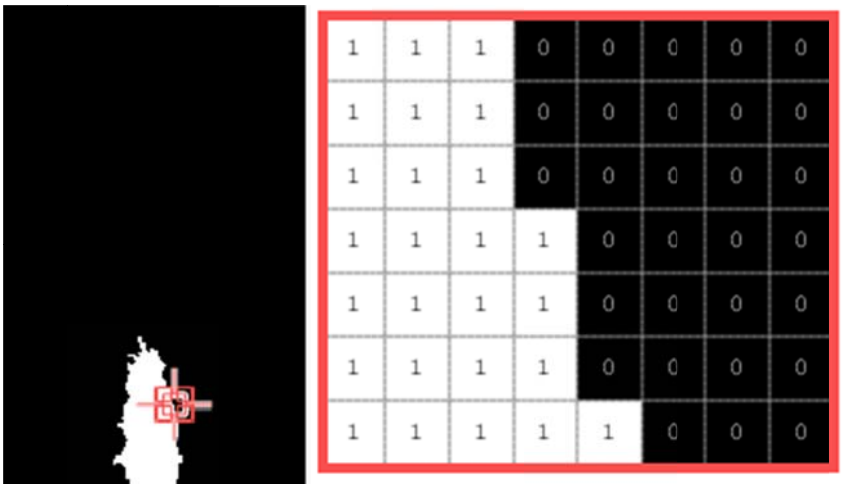

Figure 4-4. Example steam plume image and magnified region after intensity filter is applied.

4.2.5. Steam Plume Oscillation

The binary images are used to extract information about how the steam plume volume changes over time. The three major modes of oscillation are area, length, and width variation. It is worth noting that since the captured images are a two dimensional representation of a three dimensional shape, area variation related to volume variation, and length and width variation are actually related to cross sectional area variation in perpendicular planes.

Area variation over time is the simplest to obtain. The MATLAB function nnz() can be used to find the number of nonzero elements in an array and therefore the number of steam pixels in each binary image. Combining this information with the camera recording framerate results in a function of plume area [pixels] over time. An example of an area variation result for a stable steam plume over the entire 1 second of captured video is shown in Figure 4-5 and a smaller subset of time is shown in Figure 4-6.

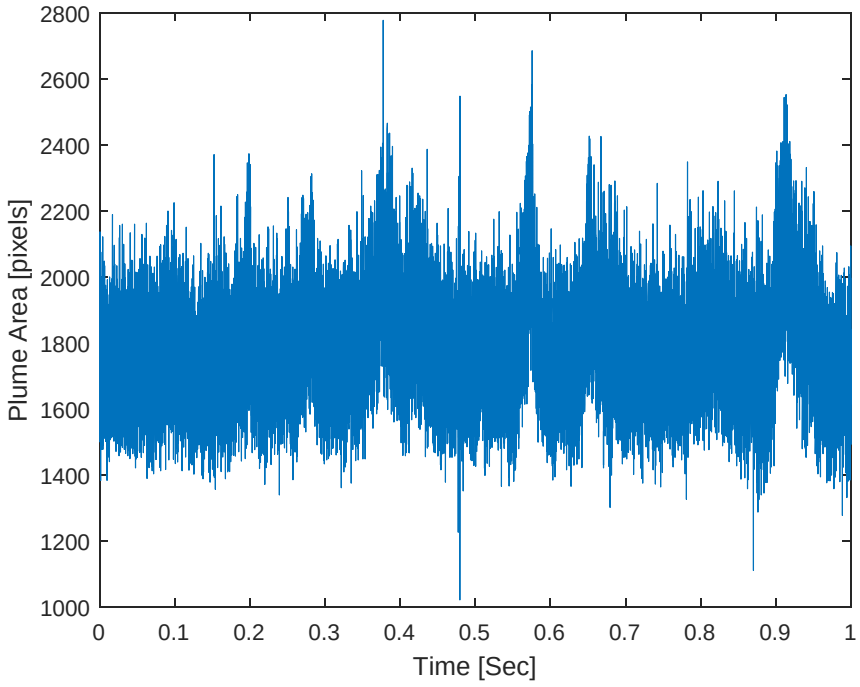

Figure 4-5. Area variation of the steam plume over the one second of video collected.

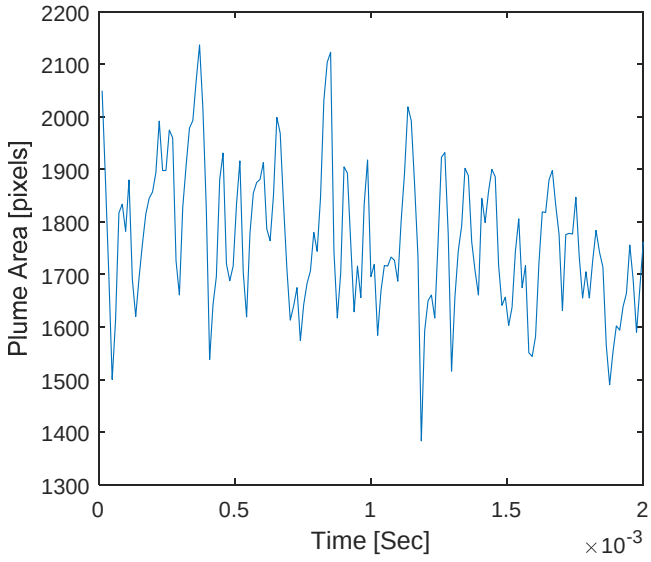

Figure 4-6. Area variation of the steam plume over a subset of time.

Length and width variation of the plume as a function of time are obtained using a similar method. In this case the nnz() function is used to count the number of steam

pixels on specified x or y lines similar to what is shown in Figure 4-7. Note that the X location is an example and actual steam plume height was measured at the center of the plume. The MATLAB function written for this purpose accepted an input vector of several x lines and y lines. The values of each group of lines were averaged to create the final function of height or width variation over time.

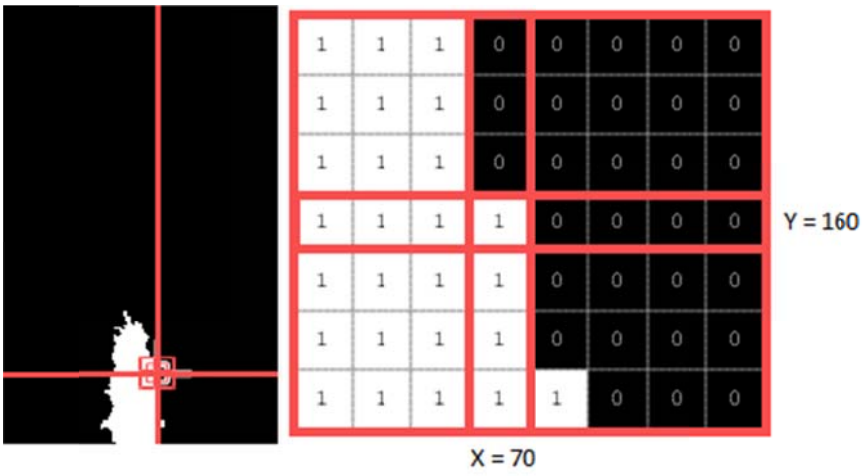

Figure 4-7. Example of the choice of x and y lines to determine length and width variation, respectively.

4.2.6. Dimensional vs. Non-dimensional Plume Oscillation

The plots shown in Figure 4-5 and Figure 4-6 give the area of the steam plume over time in the unit of pixels. The actual plume area over time can be determined using a scaled object in an image taken at the same focal point as the high speed video recording. To facilitate this, a feature of known scale (a half circle) was cut into the test section window retainer piece and the high speed camera was mounted to an indexed stage. After testing was concluded and without adjusting the focus of the lens, the camera could be moved backwards until the retainer piece cutout was in focus. The scale image could then be captured. An example of a scale image is shown in Figure 4-8.

Figure 4-8. Example scale image from testing. The half circle cutout has a diameter of 0.1875"

From the scale image shown above the relationship between pixels and an actual dimension can be obtained. In this case the half circle cutout shown is 72 pixels wide. This equates to an actual scale of 384 [pixels/inch]. The actual dimensioned value of area change is useful for purposes such as estimating the steam plume's internal pressure change using isentropic relationships as mentioned in the literature review section. However, caution must be exercised when using the variation functions with actual dimensions. The definition of the steam plume boundary is very dependent on lighting conditions and the choice of threshold value has a large effect on the calculated area. The sensitivity of the steam plume area calculation to threshold value choice is shown in Figure 4-9.

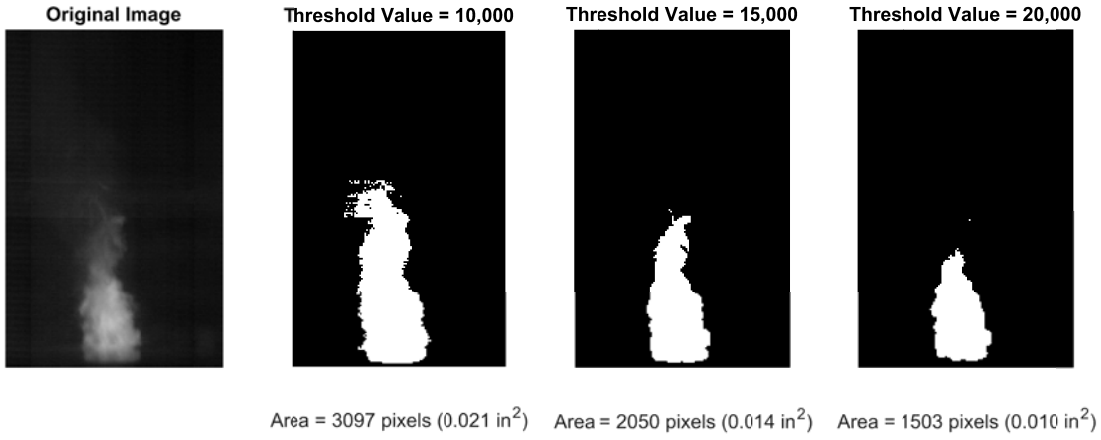

Figure 4-9. The effect of threshold value choice on calculation of plume area.

Figure 4-9 shows that the calculated plume area is highly dependent on the choice of threshold value. For this reason, only relative comparisons between steam plume oscillation magnitudes are possible and only for videos taken in succession, under the same lighting conditions, and processed with the same threshold value. Even relative comparisons of magnitude are difficult to make for videos taken on different days with small variations in the lighting conditions. For these reasons, the main feature used to compare steam plume behavior is oscillation frequency. In the next section oscillation frequency is shown to be nearly independent of threshold value choice.

4.2.7. Steam Plume Oscillation Frequency Analysis

Comparison of the plume oscillation signals directly is difficult in their raw form. However, frequency analysis can be used to understand more about the component pieces of the signals and how they correlate with observed physical behavior. The MATLAB function pwelch() was used to find the power spectrums of the plume oscillation signals. The power spectrum of a signal describes the component signal

frequencies and their magnitudes using Fourier analysis. Because the plume oscillation signals are derived from physical phenomena, the power spectrum output can be compared to the high speed videos to find the features that occur at the same frequency and therefore must be related to the specific frequency peaks. An example power spectrum from the transition regime is shown in Figure 4-10. This power spectrum calculation was performed on the function representing the width variation of the plume near the nozzle exit (plume base). The plot shown has a 150 point moving average applied to the frequency data to reduce noise and make the peak more visible; this is a common feature of most power spectrum plots in this thesis.

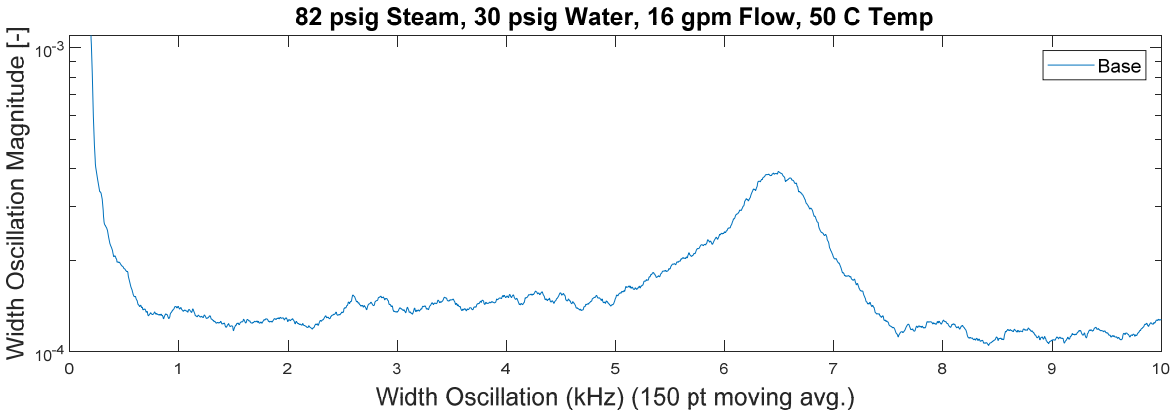

Figure 4-10. Example power spectrum from the transition regime indicating width oscillation of 6500 [Hz].

The example in Figure 4-10 shows that, in the case described in the plot title, the plume oscillates in the width direction at its base at a rate of approximately 6500 [Hz]. Examples of power spectrums produced from the other steam plume regimes are discussed in the section: Regime Descriptions. The same transition regime example can be used to illustrate two key considerations in the visual oscillation frequency analysis:

(1) the influence of the choice of spatial location where the oscillation signal is extracted from and (2) the influence of threshold value choice.

When describing the area variation of the steam plume it is obvious that the area described is simply the sum of all steam pixels in an image. However, describing the width variation of the plume is more nuanced and the choice of where along the steam plume you are talking about is non-trivial. For example, is the width variation at the base of the plume near the nozzle or at the tip of the plume and is the frequency of oscillation the same for both locations? An analysis of the influence of spatial location choice was conducted to answer this question.

Several of the video data sets were analyzed at varying distances away from the steam nozzle exit (heights). Locations were chosen in terms of fractional values of the nozzle diameter. Figure 4-11 shows an example of this study using a steam plume in the transition regime. A frame of the high speed video is shown on the left with blue lines indicating the vertical locations of the lines chosen to analyze. On the right is a plot showing a series of power spectrums of the width oscillation function determined at the locations indicated.

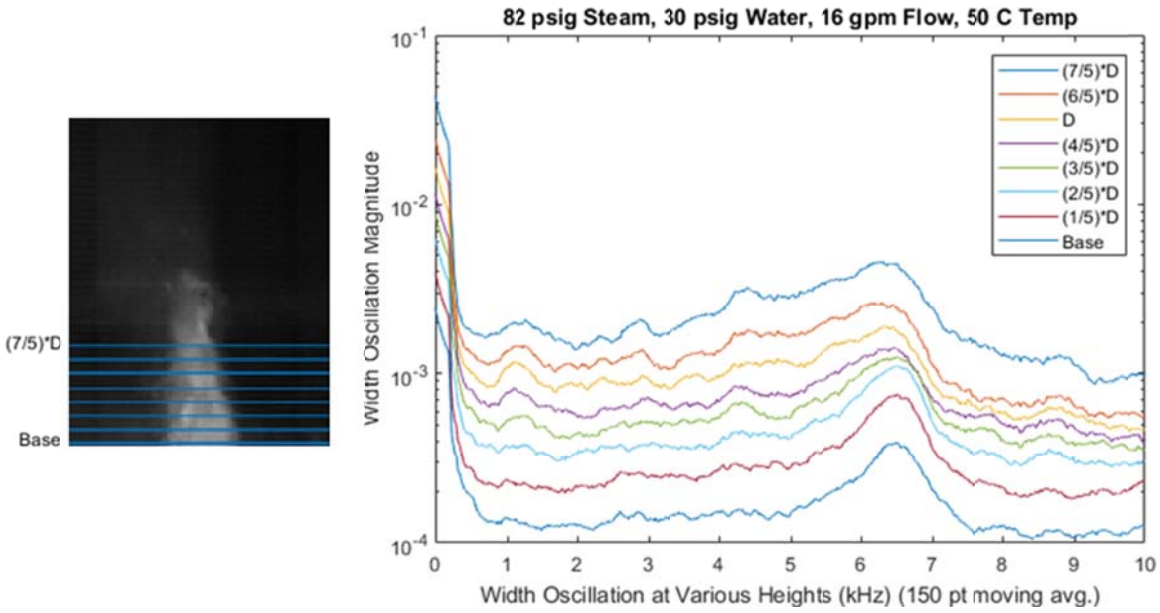

Figure 4-11. Example from the study of location choice and width oscillation frequency determination.

The plot in Figure 4-11 shows that the magnitude of width oscillation frequency is highly influenced by the height location chosen to analyze. The magnitude difference may be caused by the physical difference in width at different heights due to the tapered cone shape or other factors. Non-dimensionalizing the width variation using the average value on that line may resolve this difference, but this was not investigated. The key takeaway is that the frequency peak determined from each height location is nearly the same. In this example the frequency peak can be determined to be about 6500 [Hz] and is consistent across the height of the plume. However, Figure 4-11 shows that certain choices of height do give more or less distinct frequency peaks. The location of the most distinct frequency peak is towards the base in this example. The most distinct peak location varied between videos and so a MATLAB script was written to calculate the power spectrum of the width variation at several heights for each video in order to find

the height at which the width variation was the most distinct and could be determined most precisely.

The influence of threshold value choice on oscillation frequency determination was also studied. The result was the same: the oscillation frequency calculated was consistent regardless of the threshold value, but again the magnitude and obviousness of the peak varied. The plots in Figure 4-12 show how the power spectrums at various heights changed when the threshold value used for the intensity filter was varied between values of 10,000, 14,000, and 19,000. The plots show that the frequency peak is in the same location for each case even though the magnitude and sharpness of the frequency peak varied with intensity value.

The final consideration in this analysis is the uncertainty in oscillation frequency value. The frequency resolution output by the Fourier transform is equal to the sampling rate divided by the sample size; in this case 1 Hz (81,000 Hz / 81,000 samples = 1 Hz). However, the frequency peaks shown in Figure 4-12 have much wider distributions than 1 Hz. Even though there is generally a defined peak for each case, the sharpness of the peak varies substantially depending on location choice and threshold value used in the intensity filter. Due to these considerations, it is difficult to determine if the distribution around the frequency peak is caused by an actual variation in the oscillation frequency or if it is caused by general uncertainty in the frequency determination method. For this reason, no frequency uncertainty is defined in this thesis. Furthermore, the frequency peak sharpness varies considerably between regimes.

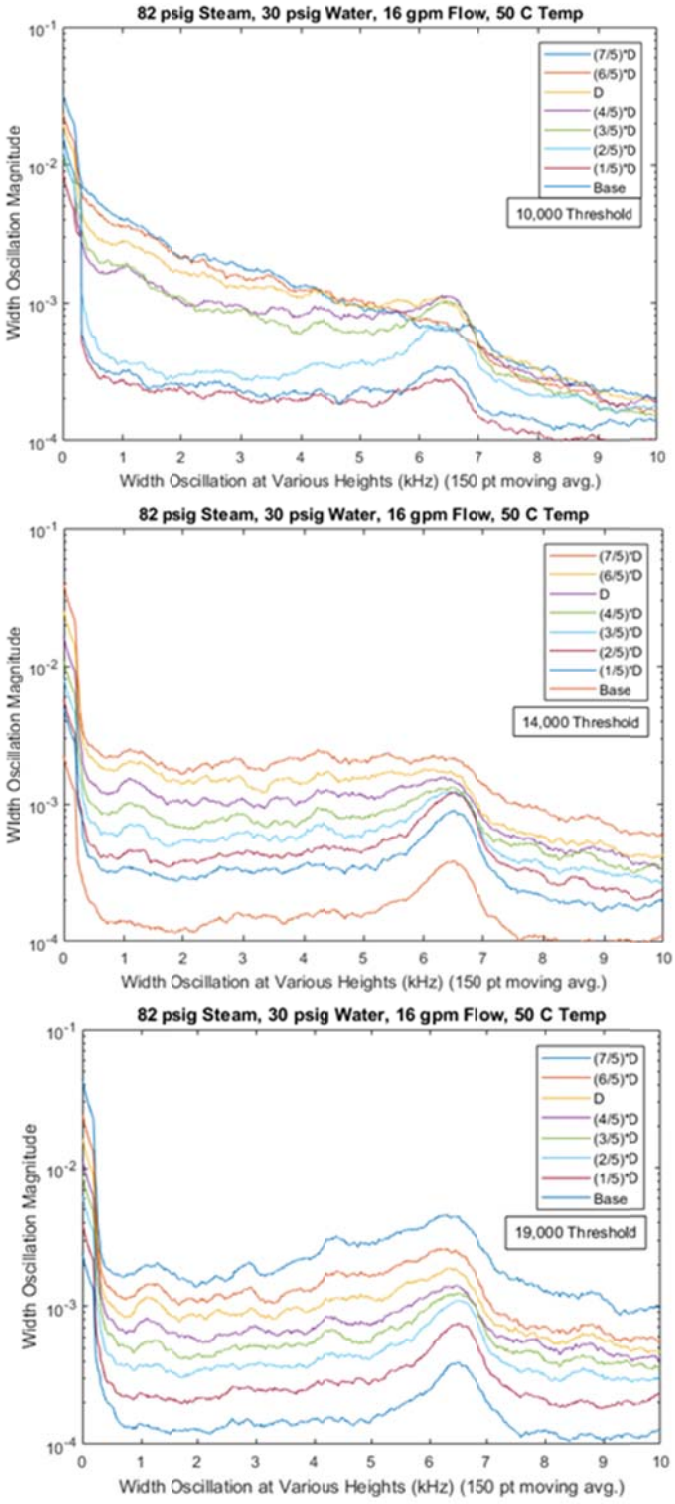

Figure 4-12. Example of the influence of intensity filter threshold value on width oscillation frequency result.

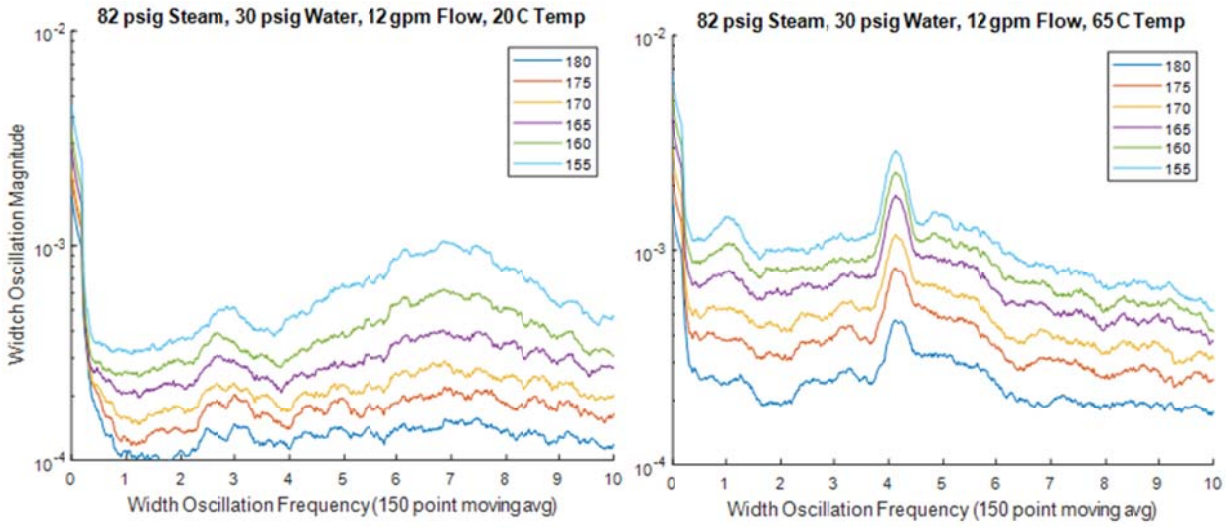

Figure 4-13. Frequency peak sharpness variation between regimes: stable (left) and transition (right).

Figure 4-13 shows how the frequency peak sharpness varies between two of the condensation regimes. There is a potential for debate about whether the sharpness of the frequency peak is due to the data processing method or due to physical behavior of the plume. The sharpness of frequency peaks is examined further in the Regime Descriptions section.

In summary, the oscillation frequency for each data point was determined by calculating the power spectrum of the oscillation signal at various spatial locations and finding the average frequency that provides maximum value. Many factors in the data processing method make determination of the exact oscillation frequency of the steam plume difficult and there is significant uncertainty in the calculated frequency. However, trends in oscillation frequency are consistent across the tests performed and they can be used to provide informative insights into the reasons why steam condensation behavior is conditionally stable or unstable.

4.3.Audio Analysis

For each data point 2 seconds of audio data was recorded using the Audio-technica microphone described previously. The audio signals were processed using the pwelch() MATLAB function to find the power spectrum in a similar way to the visual plume oscillation data. Examples of recorded audio data are presented in the Regime Descriptions section. The audio recording did not produce very interesting or easily interpreted results. The power spectrums produced were very noisy, likely due to background noise of the lab equipment and attenuation of the pressure fluctuations through the test section walls and air around the microphone. Bubble popping frequency in the unstable regime was distinguishable using the power spectrum, but the relatively small magnitude of the plume oscillations in the stable regime was indistinct. Refining the audio set-up or directly measuring water pressure fluctuations using a high speed pressure transducer is an important improvement that could be made to the experimental setup.

5. Initial, Exploratory Regime Testing

A set of tests with a broad span of process parameter values was conducted in early 2018 in order to validate the operation of the test facility and data acquisition system and to develop the data analysis methods discussed in the previous chapter. Another goal of this testing was to identify areas of interest for further study. A nozzle with a diameter 0.0935” diameter and nominal length to diameter ratio of near 1 was chosen because it is a common size used by the research sponsor. Steam pressure was fixed at 80 psig and water pressure, temperature and flow rate were each varied with high, medium, and low values. The conditions tested are shown below in Table 3.

Table 3. Initial Text Matrix from spring 2018

Water Pressure = 60 psig		Pressure Ratio = 0.765	
Water Flow Rate [L/min]	34	53	72
Water Temperatures:	20 ℃	20 ℃	20 ℃
	40 ℃	40 ℃	40 ℃
	60 ℃	60 ℃	60 ℃
Water Pressure = 45 psig		Pressure Ratio = 0.611	
Water Flow Rate [L/min]	34	53	72
Water Temperatures:	20 ℃	20 ℃	20 ℃
	40 ℃	40 ℃	40 ℃
	60 ℃	60 ℃	60 ℃
Water Pressure = 30 psig		Pressure Ratio = 0.458	
Water Flow Rate [L/min]	34.07	53	71.9
Water Temperatures:	20 ℃	20 ℃	20 ℃
	40 ℃	40 ℃	40 ℃
	60 ℃	60 ℃	60 ℃

The nozzle diameter was 0.0935” with an

The results from this initial set of tests showed

5.1.Qualitative Regime Descriptions

Previous work done in the Multiphase-Flow

5.1.1. Unstable Bubbling Condensation Regime

The existence of the unstable bubbling condensation regime is the reason for this research on direct contact condensation. The key defining characteristic in this regime is that the steam forms bubbles that pinch off from the main steam plume and collapse. The bubble formation and collapse creates pressure fluctuations and associated noise that can cause equipment damage (including to the water pressure transducer in this experiment) and horrible, loud screeching noises, which necessitate multiple layers of hearing protection during testing. An example of the unstable bubbling condensation regime is shown in Figure 5-1.

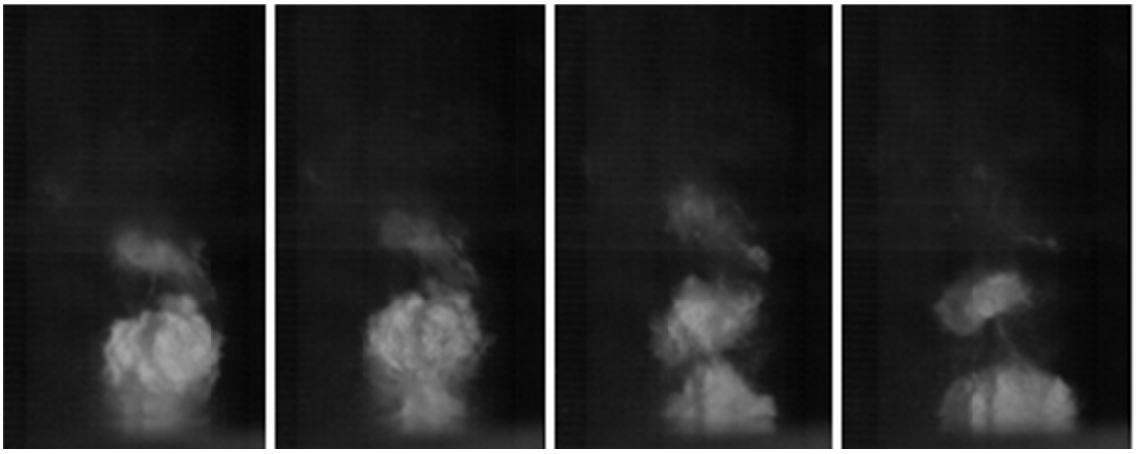

Figure 5-1. A series of images showing a bubble event in the unstable bubbling condensation regime.

5.1.2. Stable Condensation Regime

As the name implies, the stable condensation regime is the desirable operation regime for direct contact condensation equipment. The condensation process in the stable condensation regime is relatively quiet compared to the other regimes. At relatively cold water temperatures, the steam condensation noise isn't even audible over the noise of the process water pump. Figure 5-2 shows a series of images that are representative of the stable regime. Overall the steam plume is a fairly consistent cone shape.

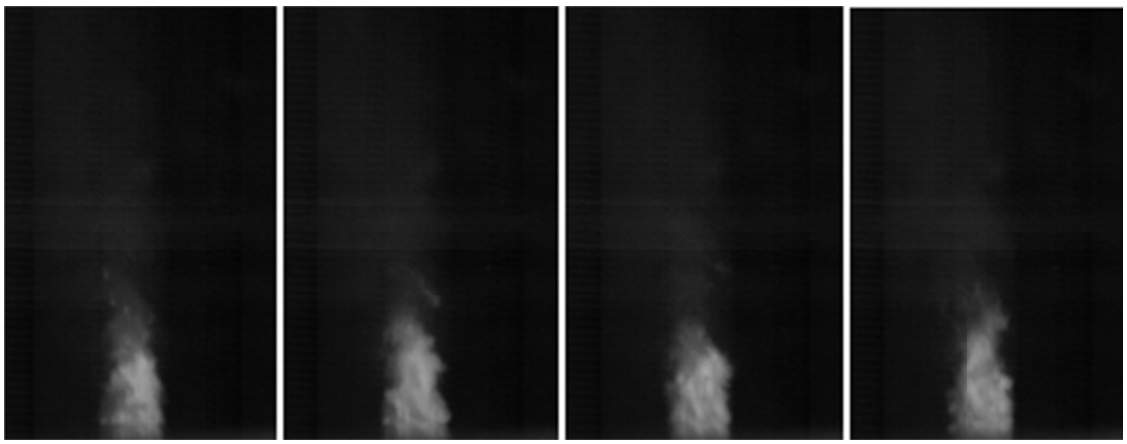

Figure 5-2. Several images representative of the stable condensation regime.

5.1.3. Condensation Oscillation Regime (Transition)

The condensation oscillation regime is the intermediate behavior between the stable condensation regime and the unstable bubbling condensation regime. The behavior in the condensation oscillation regime is characterized by less uniformity in the steam jet cone shape. The interface of the steam volume oscillates with increasing magnitude as the plume moves towards the unstable regime. Bubble-like shapes (waves) form, but no bubble separation occurs as is shown in Figure 5-3. The transition regime is another term used to describe this behavior and is explained further in chapter 6.

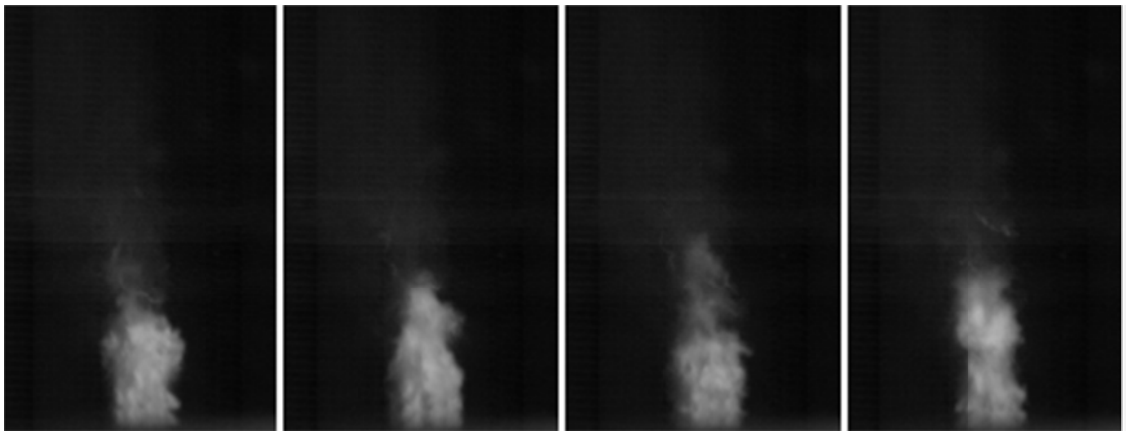

Figure 5-3. Series of images representative of the condensation oscillation regime

5.1.4. Flip-Flop Regime

The flip-flop regime was only seen in two initial test cases and to the author's knowledge has not been reported in the literature. This regime represents a combination of the condensation oscillation regime and unstable bubbling condensation regime. With no perceptible change in process conditions the condensation behavior transitions rapidly back and forth from unstable to condensation oscillation up to several times in a second. This process is best observed in the videos, but a series of representative images is shown in Figure 5-4 and a quantitative representation is discussed in chapter 6.

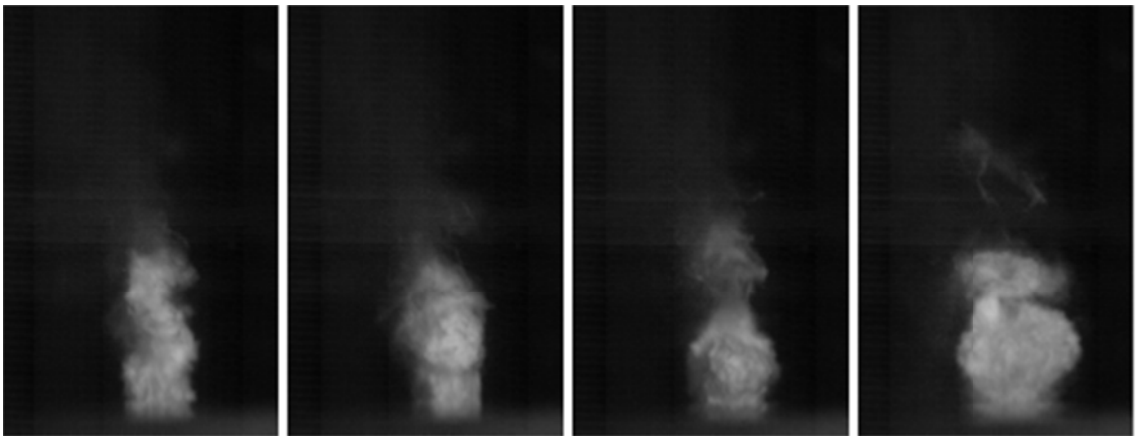

Figure 5-4. Series of images representative of the flip-flop regime.

5.1.5. Regime Map from Exploratory Regime Testing

Each of the data points in Table 3 was characterized according to the regime descriptions discussed previously. In order to compare the test data from this experiment to published literature, the regimes are plotted on a graph of water temperature vs. steam mass flux in Figure 5-5.

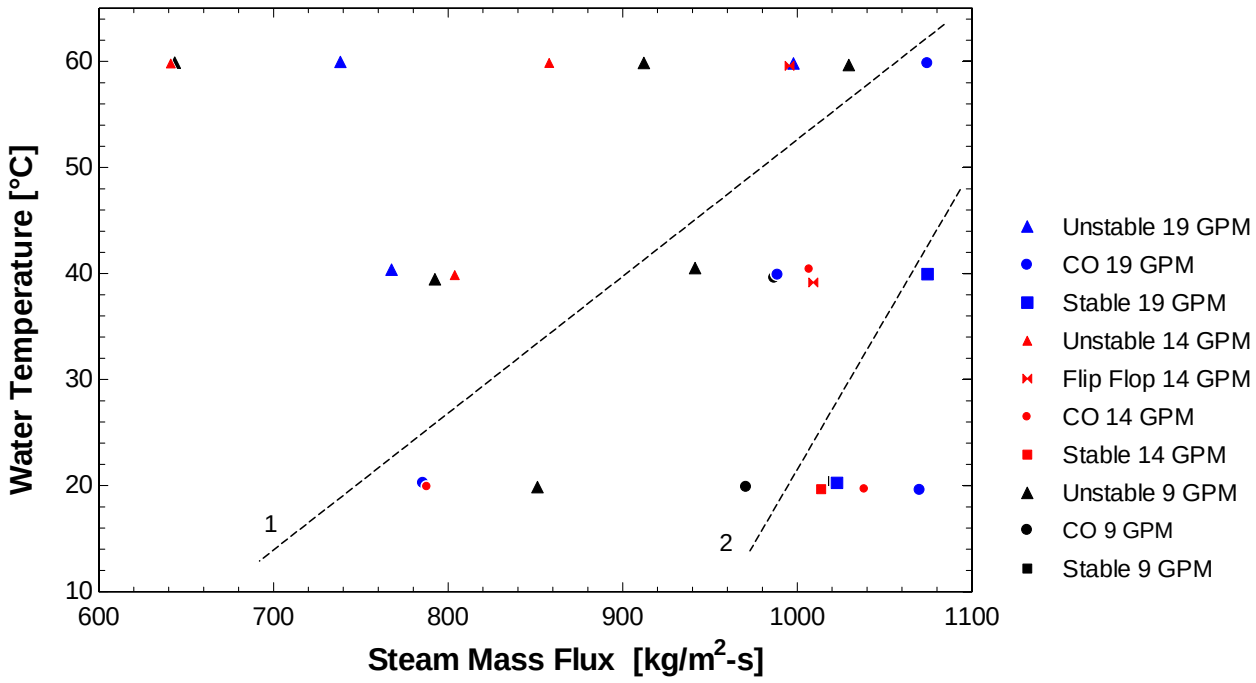

Figure 5-5. Regimes from the exploratory test matrix using similar format to published maps.

The data shown in Figure 5-5 is somewhat difficult to interpret due to the fact that the regime map data point nominal values are based on the pressure ratio between water and steam and not directly on steam mass flux. Only very general statements can be made about the behavior shown. The plume behavior is unstable at relatively low mass flux and high water temperature (to the left and above line 1). The plume behavior is generally stable at high steam mas flux and low water temperature (to the right and below line 2). The region between lines 1 and 2 contains all of the regimes and doesn't have a readily discernable pattern. A major difference between the regime map in Figure 5-5 and regime maps in literature (including Figure 2-1, Figure 2-2, and Figure 2-4) is the position of the stable regime. In almost all published regime maps the steam mass flux values in this set of experiments should result in a stable plume. The differences may

result from the simple, straight bore nozzle geometry with a short nozzle length or perhaps the trends in the other regime maps do translate well to the nozzles that are tested in this study because of their comparatively small diameter.

The asymmetrical data points are interesting relative to two important points: (1) Much published research uses mass flux as the independent variable, which is controlled by tuning a flow control valve; this indirectly sets pressure ratio and (2) Data points having the same pressure ratio do not necessarily have the same steam mass flux. The majority of previous research directly set steam mass flux and indirectly set pressure ratio to accomplish the mass flux set-point. Because mass flux was the controlled parameter, the discussion of results usually focuses on which mass flux creates which condensation regime. However, it is interesting to flip this question the other way and ask: how does condensation regime behavior affect the mass flux? Figure 5-6 shows a plot of steam mass flux vs. water to steam pressure ratio for the 9 data points at the 9 [gpm] water flow rate condition.

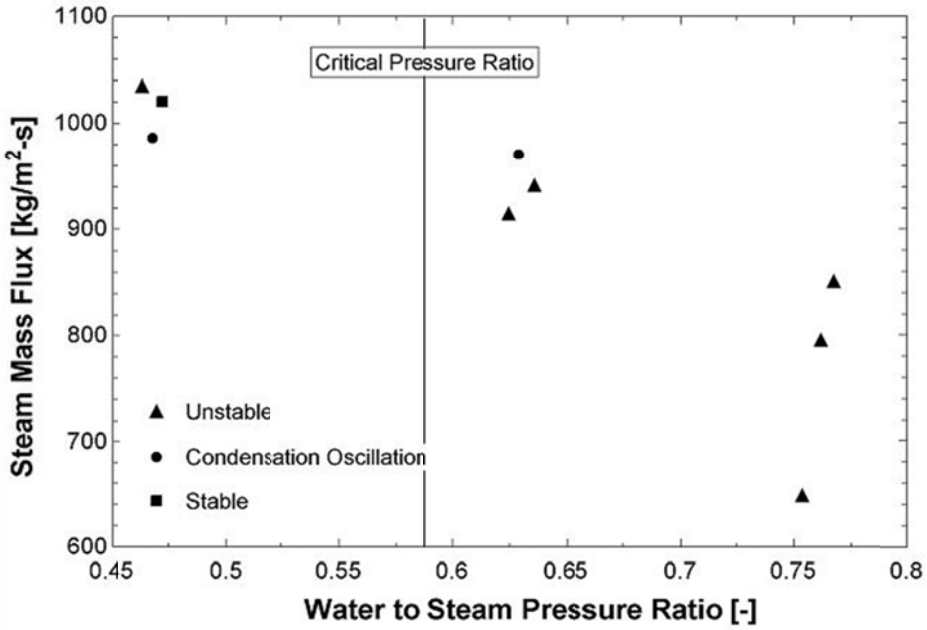

Figure 5-6. Effect of condensation regime on steam mass flux at constant average pressure ratio (9 [gpm] water flow).

In the very simple case of one-dimensional, steady, incompressible and isentropic flow of an ideal gas, the mass flow rate through a nozzle is given according to $\boldsymbol{m}=$ $\boldsymbol{A_{nozzle} * \sqrt{2 * \rho_{steam} * (P_{steam} - P_{water})}}$ Equation **1.**

$$\dot{\boldsymbol{m}} = \boldsymbol{A_{nozzle} * \sqrt{2 * \rho_{steam} * (P_{steam} - P_{water})}} \qquad \text{Equation 1}$$

This equation is derived based on assumptions that are not true in the case of direct contact condensation. The flow is not isentropic, the steam is not incompressible, and saturated steam does not behave as an ideal gas. However, the equation above is useful for examining a potential cause for the changes in mass flux. Figure 5-6 shows that for data points with equal pressure ratio the mass flux varies depending on the steam condensation regime and temperature of the water. Published literature indicates that pressure fluctuations created by the steam condensation are dependent on condensation

regime. This would indicate that the average measured pressure ratio value may be misleading. A varying pressure ratio and consequently varying steam mass flux is a major component to the explanation for the conditional instability given in the summary and is investigated further in Chapter 6.

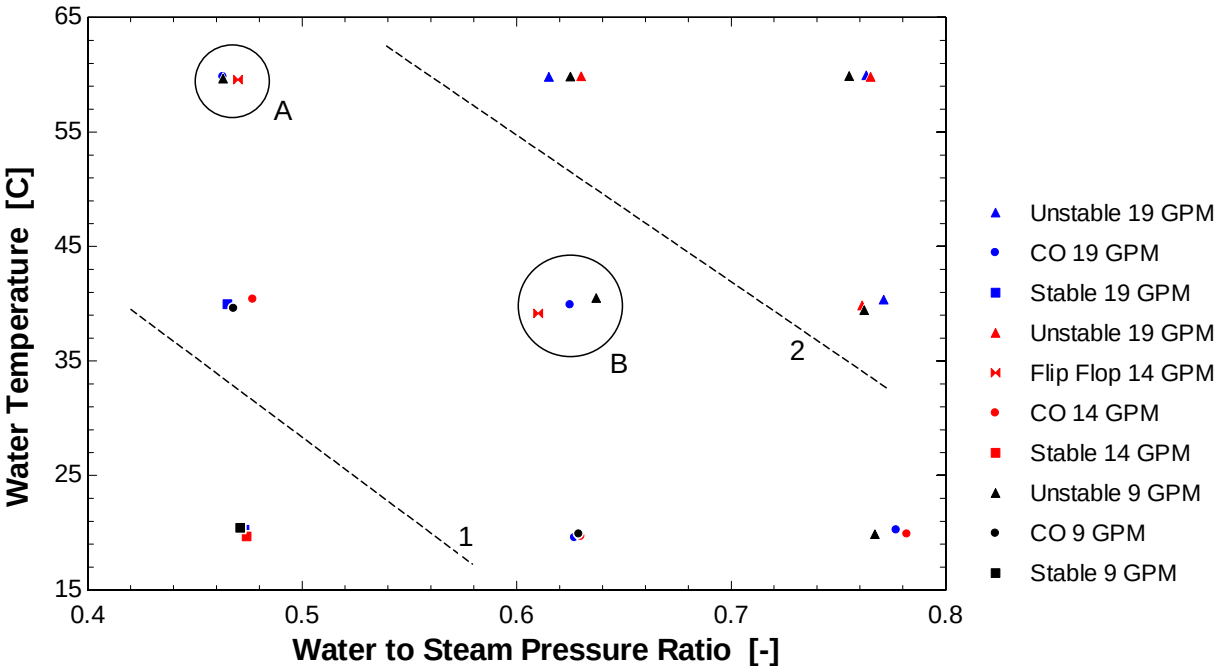

Figure 5-7. Condensation regime diagram plotted as water temperature vs. pressure ratio.

Figure 5-7 reformats the previous regime map into a map of water temperature vs. steam to water pressure ratio. This format appears more organized due to these being the set of independent parameters controlled in this testing. To the left and below line 1 the condensation behavior is stable, corresponding to low water temperature and a low pressure ratio. Above and to the right of line 2 the behavior is always unstable and this corresponds to a high water temperature and pressure ratio. The circles, A and B indicate areas of interesting behavior between lines 1 and 2. At these points the pressure ratio and

water temperature are the same, but the water flow rate changes and so does the condensation regime. It is clear that more data is needed to understand what is happening when the condensation changes regimes. The next chapter details testing conducted to understand the regime transition behavior with much higher resolution in data points.

6. Study of Stable to Unstable Transition Behavior

The initial exploratory regime map testing described in Chapter 5 provided general information on the condensation regime behavior at a series of widely spaced testing points. Based on analysis of the exploratory test results, a more detailed set of tests was planned to answer the answer the question: How can regime transition behavior be quantified? The two major behaviors analyzed here are the volume oscillation frequency of the steam plume and the mass flux variation during condensation regime transition.

A fixed pressure ratio of 0.47 was chosen for this set of experiments. This pressure ratio was the only pressure ratio from the previous testing shown in Figure 5-7 that exhibited behavior associated with all of the condensation regimes. The water flow rates chosen for testing were 12 [gpm], 14 [gpm], and 16 [gpm]. These flow rates were chosen because the 14 [gpm] case was the only flow rate in the initial exploratory study that resulted in the flip-flop regime. The water temperature was varied in increments of 5 [˚C] between 25 [˚C] and the equipment maximum of 80 [˚C] resulting in 12 temperature "steps." The combination of 1 pressure ratio, 3 flow rates, and 12 temperatures resulted in 36 data points.

In order to quantitatively compare condensation regimes, the plume volume oscillation frequency analysis method was developed with tools adapted from published literature [10], [5]. Measuring the oscillation frequency of the steam plume visually led to descriptions of pressure fluctuations created by the steam condensation and a link to oscillations of the steam and water interface as described in the literature [7]. Most published literature determines oscillation frequency of the steam plume through analysis

of measured pressure data and reference to visual frequency from videos is done qualitatively, by counting video frames. The oscillation frequencies seen in the experiments in this thesis are much higher than those in published literature (3-8 kHz in this experiment compared to 10-500 Hz in the literature) and are above the frequency resolution of most common pressure transducers. However, the Phantom V311 high-speed camera used to record the videos used in this experiment was able to capture images at high enough frequency (81 kHz) to record the oscillation frequency data visually.

Through analysis of published literature it was determined that as the water temperature increases and the condensation behavior transitions from stable to unstable there is an associated increase in the magnitude of pressure oscillations created by the plume. Experimentation with frequency analysis of the area, width and length of the plume, along with observation of the high-speed videos, indicated that analysis of the width oscillation of the plume produced the most reliable and interpretable results. All of the frequency data presented in the following sections comes from analysis of the width oscillation of the steam plume.

The area and length variation power spectra include other features not discussed here due to the difficulty associated with correlating them to observed behavior in the videos. The frequency peaks produced by the length and area frequency analysis do not exhibit consistent trends, which may be a consequence of the data analysis method. In particular, the definition of the plume length is difficult due to the tumultuous two-phase mixing region at the end of the plume. Published literature includes specific discussion on length

variation of the steam plume [11] and further analysis to investigate this using the data presented here is an opportunity for future work on this topic.

The following sections add more quantitative detail to the previously described regimes using the results of the plume width oscillation analysis.

6.1.Analytical Regime Descriptions

6.1.1. Unstable Bubbling Condensation Regime

As described previously, the unstable bubbling condensation regime is the most undesirable operating regime for the direct contact condensation. The bubble formation and collapse that characterizes this regime creates large, high frequency pressure fluctuations and associated screeching noises. An example of a bubble separation event is shown in Figure 6-1.

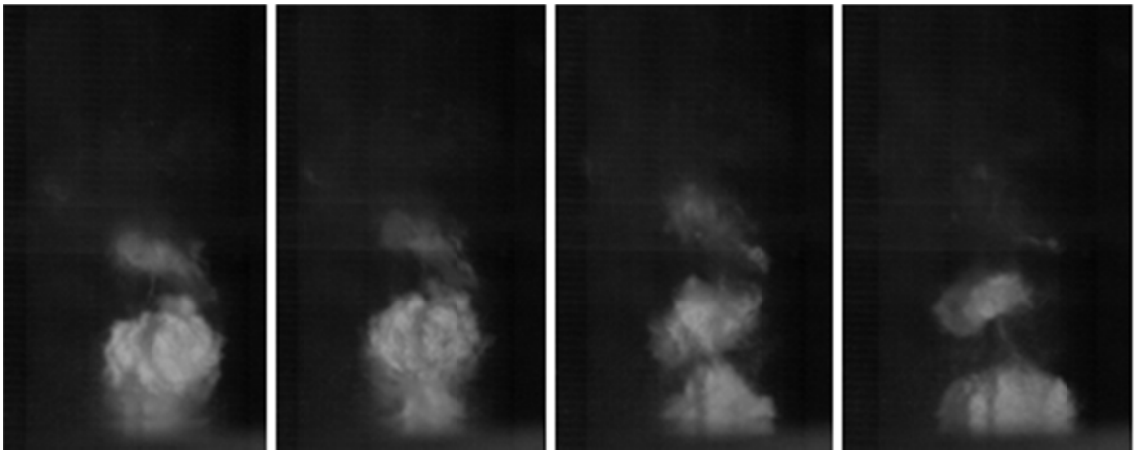

Figure 6-1. Series of images from the unstable bubbling condensation regime.

The bubble formation creates an approximately sinusoidal signal when plotting the width magnitude along a single horizontal line over time (frame number), as shown in Figure 6-2. Each period of the sinusoid represents a bubble passing through the

horizontal line. As the figure indicates, the bubble size isn't consistent and this is also observed in the videos. Beginning at frame number 0 the bubble is not seen on the line. As the bubble moves upward the signal grows in magnitude until it reaches a peak indicating the center of the bubble. The signal decreases in magnitude as the bubble continues to rise and eventually passes the vertical position of analysis, returning the function to its minimum which is near frame 46 in this case, and the cycle repeats. This plot includes 1000 frames and at 81,000 [Hz] sampling frequency this represents 24.7 [ms] of time. 49 periods are seen in this plot and this would indicate that a bubble event happens approximately every 0.5 [ms] (i.e., at 2000 [Hz]).

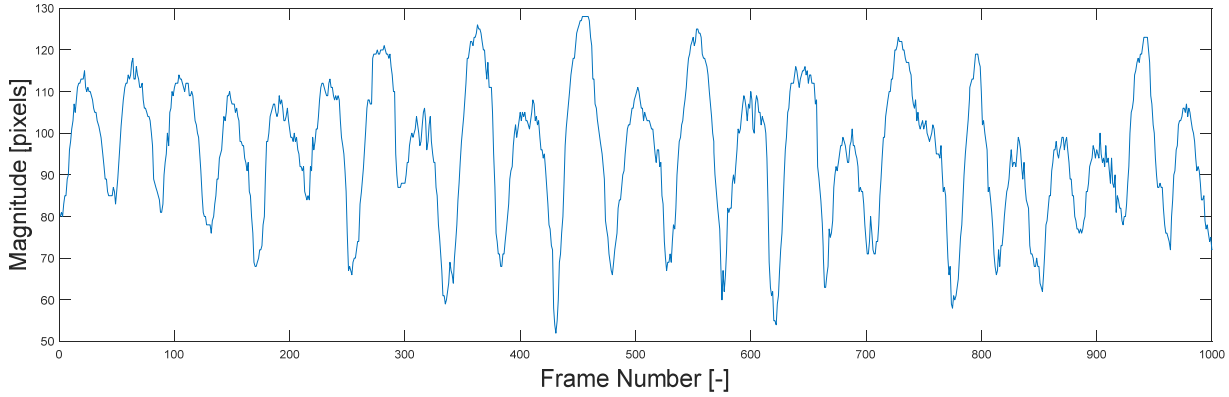

Figure 6-2. Width oscillation along a horizontal line where the bubble separation occurs.

The power spectrum associated with the unstable bubbling condensation case above indicates a calculated bubble separation frequency of 2047 [Hz]. Figure 6-3 shows a characteristic power spectrum plot from the unstable regime. Two obvious frequency peaks are always present on the power spectra. The first peak represents the frequency of the bubble separation. The second peak is always exactly twice the frequency of the bubble separation frequency.

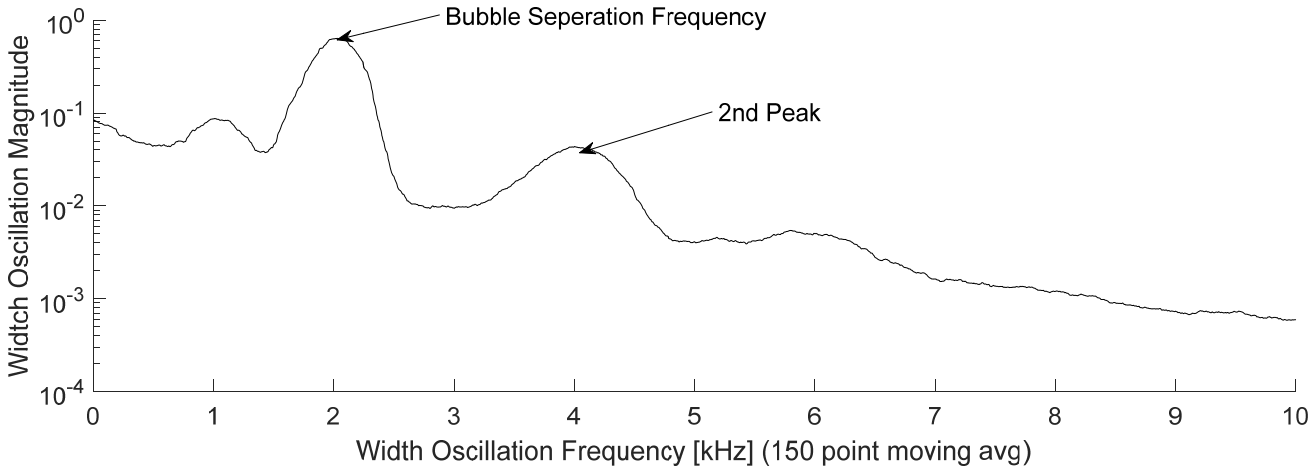

Figure 6-3. Power spectrum plot from the unstable bubbling condensation regime.

6.1.2. Stable Condensation Regime

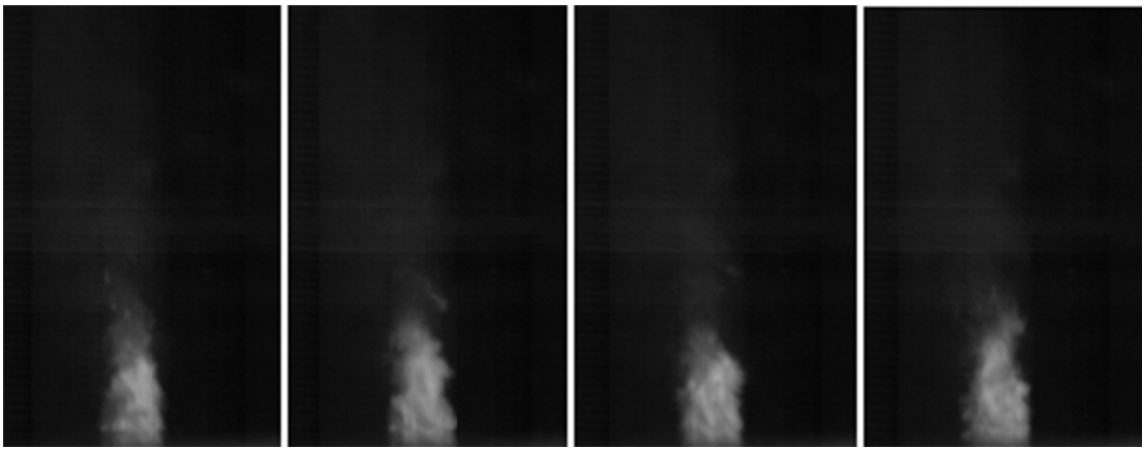

Figure 6-4. Characteristic images from the stable condensation regime.

The stable condensation regime is characterized by a consistent cone shape that doesn't change in volume by an appreciable amount when observed visually as shown in Figure 6-4. However, the oscillation frequency analysis technique allows for more information to be derived from the videos than can be obtained through simple visual

analysis. A power spectrum of the width oscillation frequency of the plume in the stable condensation regime is shown in Figure 6-5. Two important characteristics are presented here and related to the frequency peak sharpness. (1) The relative flatness and non-smoothness of the distribution makes the peak determination somewhat uncertain in this regime. (2) There is a relatively large distribution of frequencies that contribute to the peak when compared to the unstable bubbling condensation regime

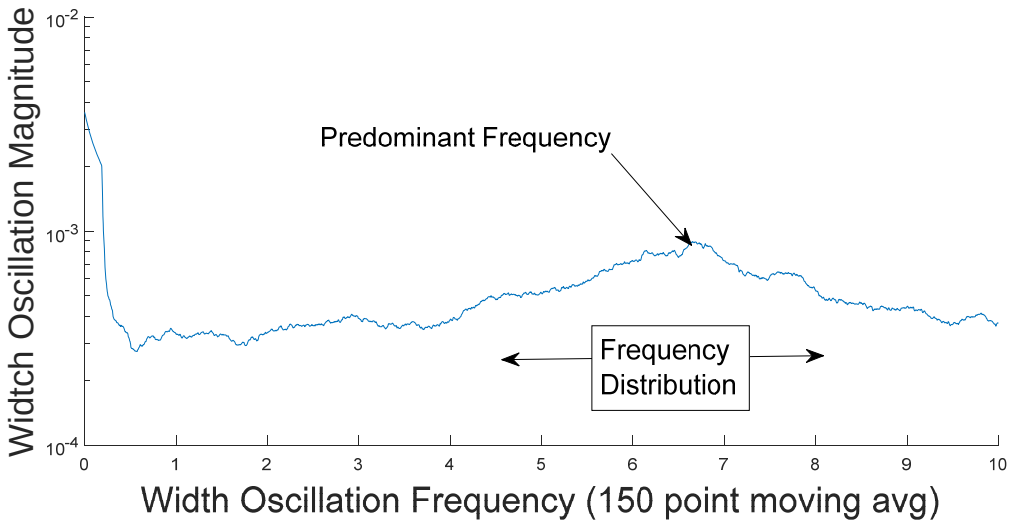

Figure 6-5. Power spectrum from the stable condensation regime.

This distribution of frequencies is likely due to the somewhat random oscillation behavior of the steam plume in this regime and this characteristic contributes to the stability. Pressure fluctuations occurring at a range of frequencies are less likely to become in phase and amplify each other. The distributed frequencies are clustered around a predominant frequency that generally decreases with increasing water temperature as discussed later in this chapter. The oscillation magnitude has no perceptible change with water temperature in this regime.

6.1.3. Condensation Oscillation (Transition) Regime

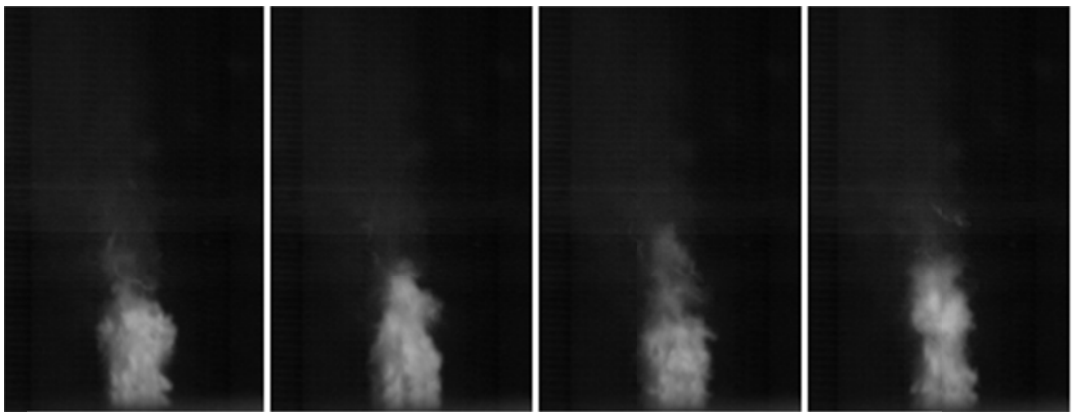

Figure 6-6. Series of images representative of the condensation oscillation regime.

The condensation oscillation regime is characterized by less uniformity in the steam jet cone shape compared to the stable regime. The oscillation frequency analysis method allows for a more quantitative description of the frequency behavior as condensation potential decreases in this regime. In general, the oscillation behavior of the plume in the condensation oscillation regime increases in magnitude and decreases in frequency with increasing water temperature. The frequency change with temperature is much more apparent in this regime compared with the stable regime and power spectra at a series of water temperature values is shown in Figure 6-7 to exhibit this behavior. Note that the frequency reduction that occurs with increasing water temperature is always clear in the power spectra, but the magnitude trend shown here is not as distinct in the other flow rate cases.

Another important characteristic of the power spectra in Figure 6-7 is that the frequency peak that is present in the width oscillation signal is much sharper when compared to the frequency peak seen in the stable oscillation regime. The sharpness of

the peak indicates that the plume oscillation is occurring at a more consistent and less distributed frequency value. Furthermore, Figure 6-7 appears to indicate that the power spectra frequency peak becomes increasingly sharp with increasing water temperature. The collapsing of the oscillation frequency to a more defined value with higher magnitude contributes to the explanation of regime transition based on high frequency variation of pressure ratio mass flux as discussed in a later section.

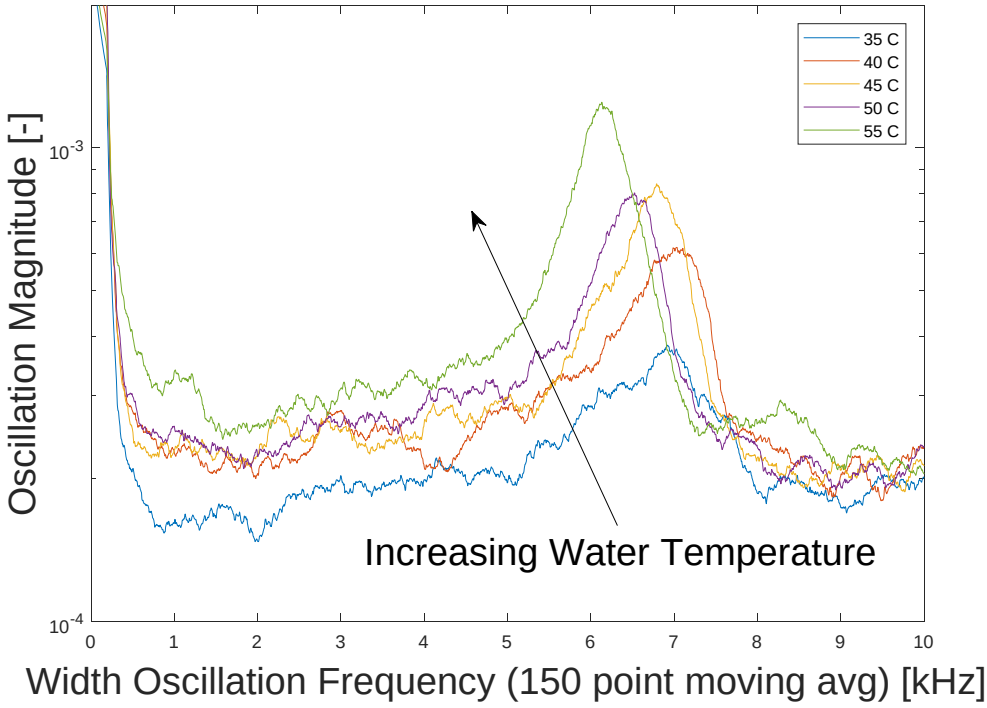

Figure 6-7. Power spectrum of the width oscillation in the condensation oscillation regime for the 16 [gpm] case showing increasing magnitude and decreasing frequency with increasing water temperature.

6.1.4. Flip-flop Regime

The flip-flop regime exhibits a combination of the condensation oscillation regime and unstable bubbling condensation regime. With no perceptible change in process conditions the condensation behavior transitions rapidly back and forth from unstable

bubbling condensation behavior to condensation oscillation behavior at rate of up to several times in a second. This behavior is seen clearly on a plot of plume width vs. time as shown in Figure 6-8.

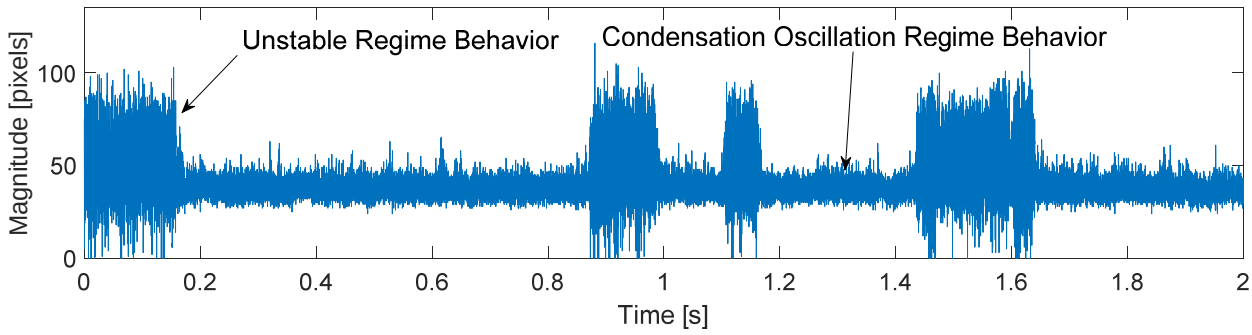

Figure 6-8. Width oscillation vs. time for a characteristic flip-flop regime example.

Figure 6-8 shows the distinct difference in plume oscillation magnitude of the unstable bubbling regime and the condensation oscillation regime. The figure also illustrates the very rapid transition between each regime and the frequency at which the transition happens. In this example, the plume behavior is in the bubbling condensation regime for an approximate total of 0.5 seconds and in the condensation oscillation regime for an approximate total of 1.5 seconds. The relative “duty cycle” of the time spent in each regime varies over test cases in the flip-flop regime and there are not enough data to draw definitive conclusions about it. A zoomed in portion of the data from Figure 6-8 is shown in Figure 6-9 to highlight the transition between regime behaviors.

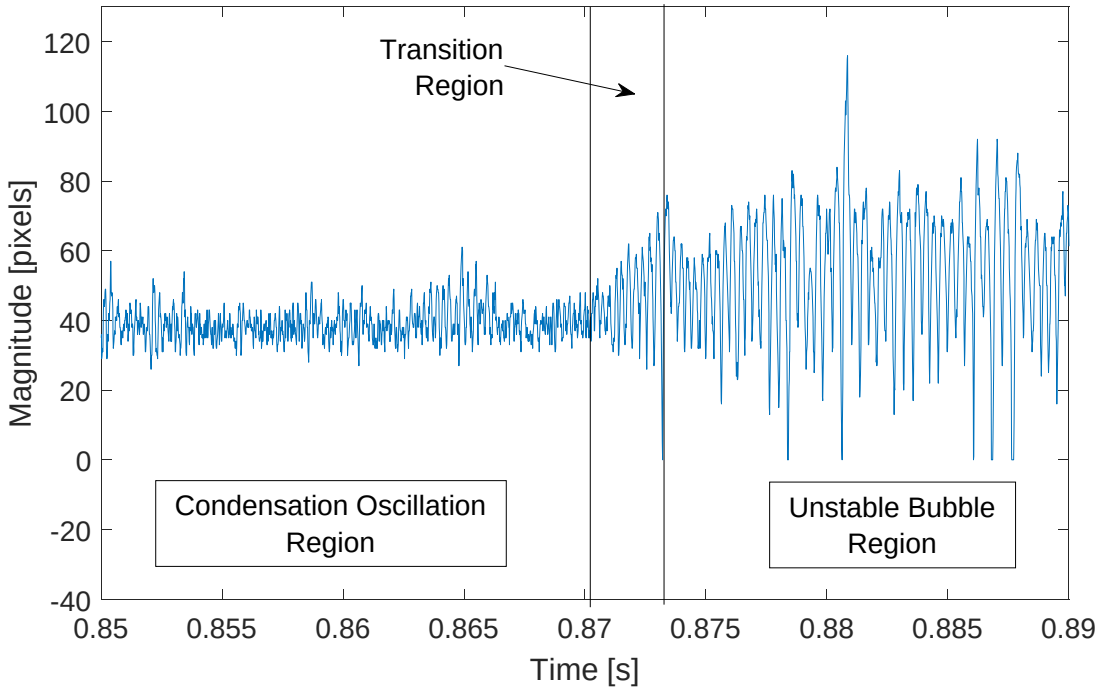

Figure 6-9. Zoomed in portion from Figure 6-8 showing the transition region between regime behaviors.

Figure 6-9 illustrates the rapid regime transition. In this example the transition region indicated occurs over approximately 3 [ms]. During approximately 10 cycles of oscillation, the magnitude of the oscillation increases rapidly and unstable bubble formation behavior is observed. By isolating the sections of data representing each regime the oscillation frequency of both behaviors can be determined as shown in Figure 6-10.

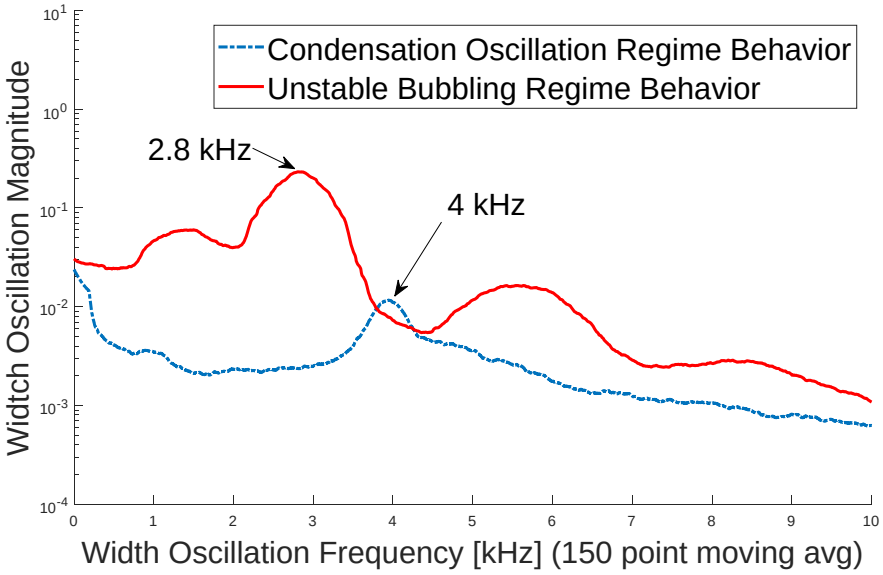

Figure 6-10. The difference in width oscillation frequency and bubble formation frequency when the two behaviors are isolated in a flip-flop regime example.

6.1.5. Oscillation Frequency Behavior during Regime Transition

Combining the oscillation frequency analysis discussed in the preceding sections leads to the observation of a clear trend in the oscillation behavior that is summarized in Figure 6-11.

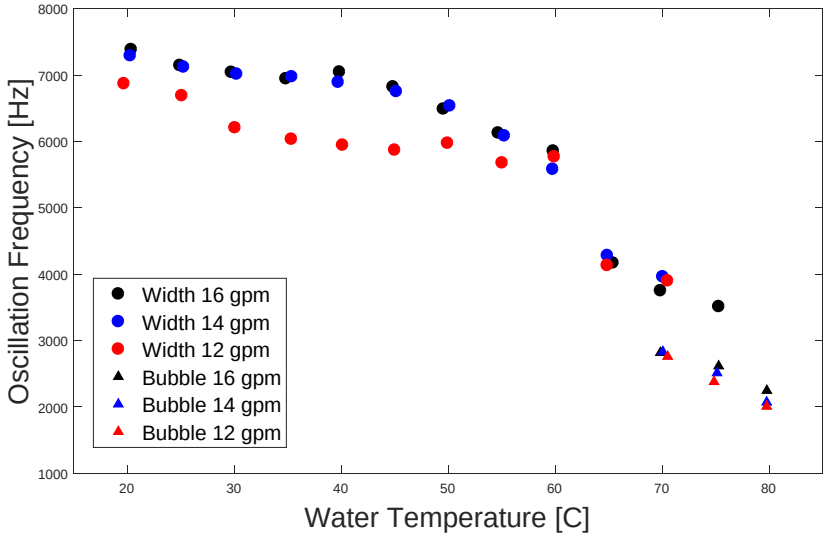

Figure 6-11. Oscillation frequency as a function of increasing water temperature for all data cases.

As seen in Figure 6-11, the trend of decreasing oscillation frequency with increasing water temperature is clearly observed. However, the effect of changing water flow rate is unclear. The change in magnitude of the water flow rate between the 12, 14, and 16 [gpm] cases likely changes the frequency by an amount that is too small relative to the uncertainty in the oscillation frequency to create discernable differences. This result matches the result seen by Simpson and Chan that pressure oscillation frequency increases with increasing pool subcooling [6].

6.1.6. Mass Flux Behavior during Regime Transition

Figure 2-1Figure 6-12 shows the variation in steam mass flow vs. water temperature. In general, the mass flux tends to decrease by about 10% as the steam plume transitions from the condensation oscillation regime to the unstable bubbling regime between approximately 60 [˚C] and 75 [˚C]

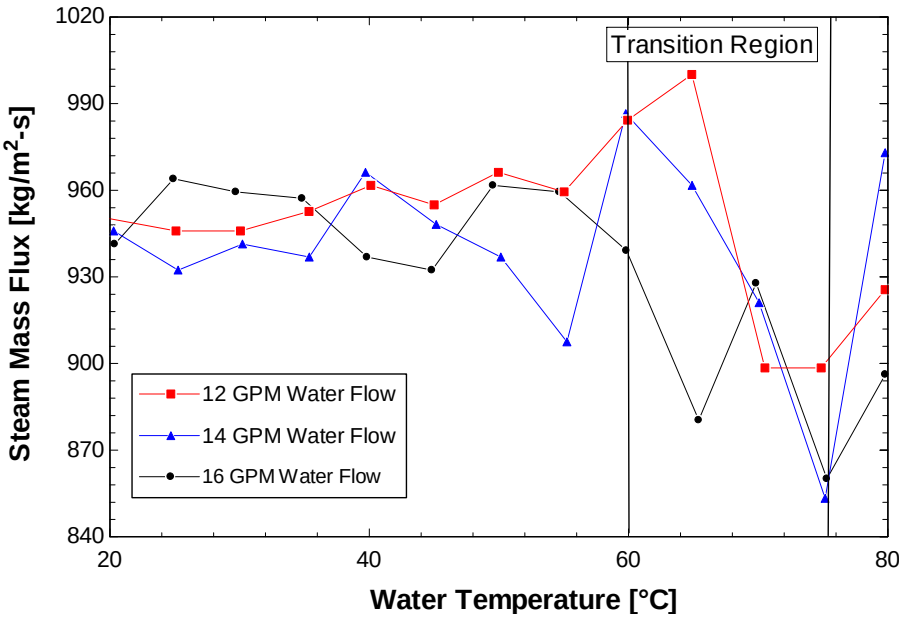

Figure 6-12. Steam mass low rate vs. water temperature showing the decreasing mass flow rate during the transition to the unstable bubble separation regime.

6.1.7. Regime Map from the Study of Stable to Unstable Transition Behavior

A map of the condensation regimes seen during the study of stable to unstable transition is shown in Figure 6-13. The regime transition behavior follows the trends discussed earlier. At low water temperature the condensation behavior is stable. As water temperature increases the steam and water interface oscillates with increasing magnitude and decreasing frequency in the transition (condensation oscillation regime). As water temperature increases further the plume presents as the flip-flop regime and the steam condensation transitions between condensation oscillation behavior and unstable bubble formation behavior. At high water temperatures the plume continuously forms bubbles that separate and detach from the main body.

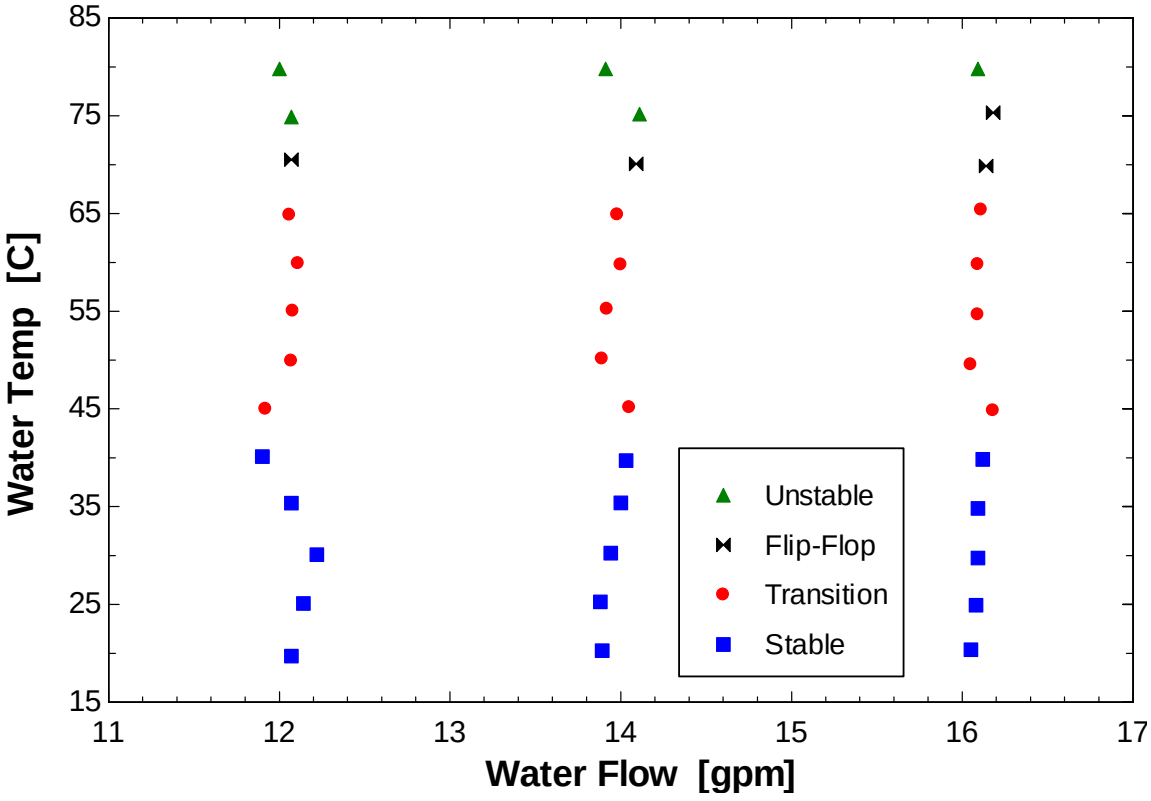

Figure 6-13. Regime map result from the study of stable to unstable regime transition.

7. Summary and Conclusions

During direct contact condensation of steam in water crossflow oscillations of the steam plume volume create water pressure fluctuations and associated audible noise. Initial testing focused on evaluating the performance of the test facility and gaining an understanding of condensation behavior at a wide variety of parameter values. Further testing was conducted to understand how the oscillation frequency and magnitude changed during condensation regime transition by varying water temperature and water flow rate at a single pressure ratio. The analysis resulted in trends that qualitatively matched other published results, but differed quantitatively, which was likely due to differences in the geometry of the steam nozzle used in the experiment and the effect of crossflowing water.

7.1.Comparison to Regime Maps in Literature

Comparison of the regime map from this thesis with those discussed in the background chapter results in general qualitative agreement. The regime map from Cho et al. is referenced most frequently in the literature. The data presented in chapter 6 used a fixed water-to-steam pressure ratio, fixed water flow rate, and varying water temperature. Since the fixed water-to-steam pressure ratio produced generally constant mass flux the trend in measured data from this set of experiments can be roughly represented by the arrow indicated in Figure 7-1 overlaid on the regime map from Cho et al. [12]. Note that the mass flux values measured in this set of experiments were much different than from Cho and the arrow placement is not representative of the true measured values (indicated in Figure 6-12). However, very similar trends in regime

behavior are observed related to the transition between stable condensation (SC), condensation oscillation (CO), and bubbling condensation oscillation (BCO) with increasing water temperature.

Starting at low water temperature the plume behavior is in the stable regime. As water temperature increases and reaches about 40 [˚C] the behavior changes to the condensation oscillation regime. As water temperature increases further to around 80 [˚C] the condensation behavior is in the bubbling condensation oscillation regime. This trend shows good agreement with the trends in Figure 6-13. The shift in mass flux at which the trend occurs is possibly due to the influence of flowing water present in this experiment and not Cho's.

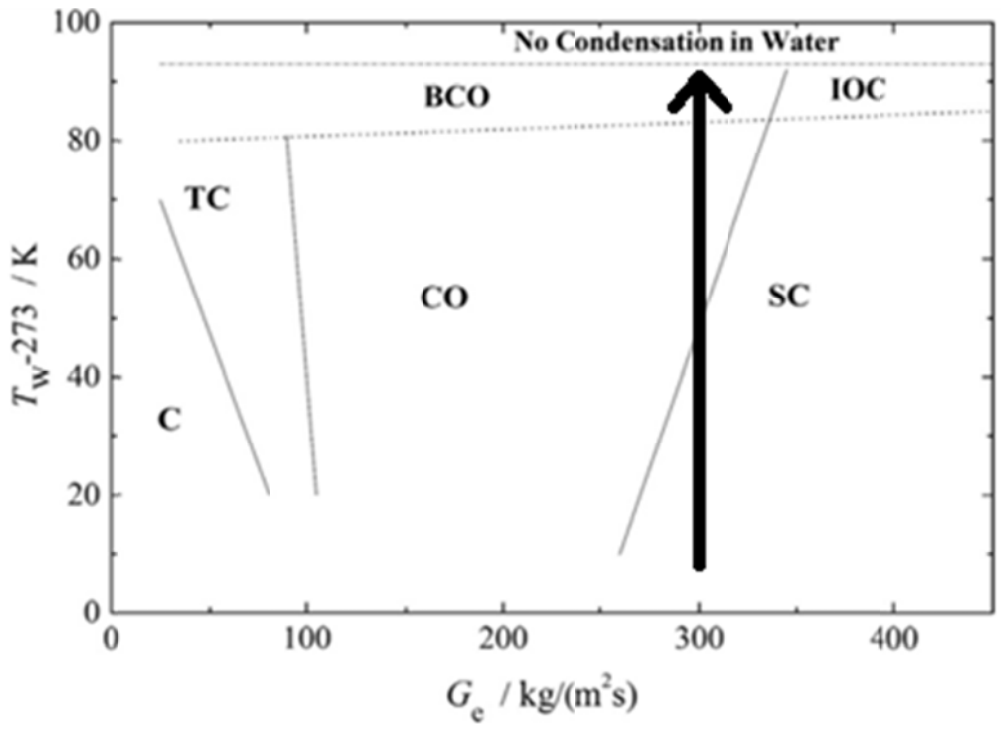

Figure 7-1. Trends in the regime map from Cho et. al are in general agreement with the thesis results.

7.2.Change in Plume Volume Oscillation Frequency during Regime Transition

The oscillation frequency change during regime transition is summarized in Figure 7-2. In the stable condensation regime the plume volume oscillates rapidly and somewhat randomly over a large distribution of frequencies. The predominant frequency is centered about a value that is relatively unchanged with changes in water temperature. This condensation regime behavior doesn't produce much noise because the volume fluctuations are relatively small in magnitude and spread over a range of frequencies. As water temperature is increased, the condensation behavior changes to the condensation

oscillation regime. The steam plume volume oscillates with greater magnitude and lower frequency as water temperature is increased. The increase in plume oscillation volume creates increased pressure fluctuation magnitude and louder noise. In this regime the oscillation frequency collapses onto a more defined value. Bubble-like waves are created along the steam plume in this regime, but do not break off of the main plume body.

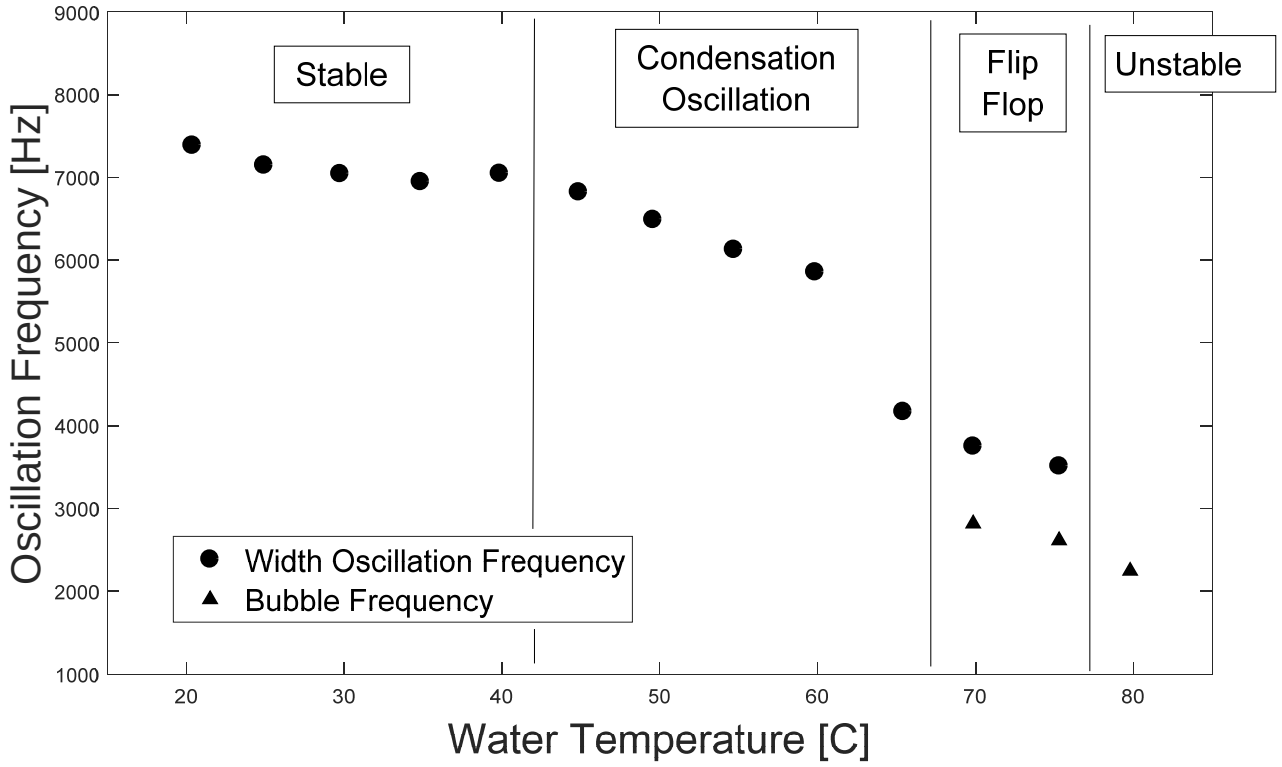

Figure 7-2. Oscillation frequency vs. water temperature for the 14 [gpm] case highlighting frequency behavior in the different condensation regimes

At very high water temperature, the condensation behavior is unstable and large steam bubbles separate from the main steam volume and collapse. The bubble collapse events create large pressure fluctuations and very loud and uncomfortable screeching noise at several kHz. As water temperature increases further the frequency of bubble

separation decreases. Between the condensation oscillation regime and unstable condensation regime there is a regime where the steam behavior quickly alternates from condensation oscillation behavior to unstable bubble separation behavior and this is termed the flip-flop regime. This regime is seen visually and is audibly recognized by a "chirping" noise where the chirps represent the portion in the unstable bubbling regime. To the author's knowledge this regime has not been reported in the literature.

7.3. Proposed Explanation for Plume Volume Oscillation and Frequency Behavior

A general explanation for the plume oscillation instability is proposed here based on two key ideas:

(1) The steam mass input rate is mainly controlled by the water-to-steam pressure ratio. The pressure ratio is influenced by pressure oscillations in the water that are induced by plume volume change.

(2) The condensation rate of steam at the steam/water interface is mainly controlled by the condensation potential of the water and the surface area of the steam plume.

Oscillations in the steam plume volume are created by an imbalance in the rate of steam mass input to the plume and the condensation rate of steam at the plume boundary. The condensation potential of the water is large at low water temperature and high water flow rate. The condensation rate can be roughly represented by a heat transfer rate given by the surface area of the plume multiplied by a convection coefficient and temperature difference between the steam and water. Condensation rate increases with an increase in surface area, an increase in the convection coefficient (higher water flowrate), or an

increase in temperature difference. Beginning with a case of large condensation potential, the plume behavior is stable and quiet. If the steam input rate is slightly higher than the steam condensation rate then the plume volume grows a little larger, which increases surface area and thus condensation rate. This increase in volume increases the local pressure ratio by increasing local water pressure [9] this decreases the steam input rate. Due to the high condensation potential of the water the magnitude of these fluctuations is kept small.

As the condensation potential of the water decreases the steam plume surface area must grow increasingly larger to create enough increase in condensation rate to counter an imbalance in steam input rate, which also takes longer. The decreasing condensation potential creates increasingly larger and slower oscillations in steam plume volume. The increasing plume oscillation magnitude generates increasingly louder noise. At some critical frequency or amplitude the oscillations become large enough that vortex rotation behavior at the plume edge draws liquid water from the base of the plume into itself and bubbles pinch off from the main steam plume and collapse creating loud screeching noise.

References

[1] C. P. Greef, “A study of the condensation of vapor jets injected into subcooled liquid pools,” *Gen. Electr. Gener. Board, Berkeley Nucl. Lab.*, 1975.

[2] P. Kerney, G. Faeth, and D. Olson, “Penetration Characteristics of a Submerged Steam Jet,” vol. 18, no. 3, pp. 548–553, 1972.

[3] V. Barot, “Thermal and Fluid Behavior of a Steam-Driven Jet in Subcooled Water Crossflow,” 2011.

[4] C. K. Chan and C. K. B. Lee, “A regime map for direct contact condensation,” *Int. J. Multiph. Flow*, vol. 8, no. 1, pp. 11–20, 1982.

[5] Q. Xu, L. Guo, and L. Chang, “Interfacial characteristics of steam jet condensation in crossflow of water in a vertical pipe,” *Appl. Therm. Eng.*, vol. 113, pp. 1266–1276, 2017.

[6] M. E. Simpson and C. K. Chan, “Hydrodynamics of a Subsonic Vapor Jet in Subcooled Liquid,” *J. Heat Transfer*, vol. 104, no. May 1982, p. 271, 1982.

[7] H. Nariai and I. Aya, “Fluid and pressure oscillations occuring at direct contact condensation of steam flow with cold water,” *Nucl. Eng. Des.*, vol. 95, no. C, pp. 35–45, 1986.

[8] B. Qiu, J. Yan, D. Chong, and S. T. Revankar, “Experimental investigation on the mechanism of pressure oscillation for steam jet in stable condensation region,” *Exp. Therm. Fluid Sci.*, vol. 82, pp. 1–7, 2017.

[9] J. Tang, C. Yan, L. Sun, Y. Li, and K. Wang, “Effect of liquid subcooling on acoustic characteristics during the condensation process of vapor bubbles in a subcooled pool,” *Nucl. Eng. Des.*, vol. 293, pp. 492–502, 2015.

[10] Q. Xu, L. Guo, S. Zou, J. Chen, and X. Zhang, “Experimental study on direct contact condensation of stable steam jet in water flow in a vertical pipe,” *Int. J. Heat Mass Transf.*, vol. 66, pp. 808–817, 2013.

[11] B. Qiu, S. Tang, J. Yan, J. Liu, D. Chong, and X. Wu, “Experimental investigation on pressure oscillations caused by direct contact condensation of sonic steam jet,” *Exp. Therm. Fluid Sci.*, vol. 52, pp. 270–277, 2014.

[12] S. Cho, C. . Song, and C. . Park, “Experimental study on dynamic pressure pulse in direct contact condensation of steam jets discharging into subcooled water,” *At. Energy Soc. Japan*, vol. 529, pp. 291–298, 1998.